Installation and Performance Testing of Solar Air Heater for Office Heating

Khaled Alteer

Submitted to the
Institute of Graduate Studies and Research
in partial fulfillment of the requirements for the degree of

Master of Science
in
Mechanical Engineering

Eastern Mediterranean University
January 2017
Gazimağusa, North Cyprus

Approval of the Institute of Graduate Studies and Research

_____
Prof. Dr. Mustafa Tümer
Director

I certify that this thesis satisfies the requirements as a thesis for the degree of Master of Science in Mechanical Engineering.

_____
Assoc. Prof. Dr. Hasan Hacışevki
Chair, Department of Mechanical Engineering

We certify that we have read this thesis and that in our opinion it is fully adequate in scope and quality as a thesis for the degree of Master of Science in Mechanical Engineering.

_____
Asst. Prof. Dr. Murat Özdenefe
Supervisor

Examining Committee
_____

1. Prof. Dr. Uğur Atikol   _____

2. Prof. Dr. Fuat Egelioğlu   _____

3. Asst. Prof. Dr. Murat Özdenefe   _____

ABSTRACT

A widespread development has been occurred in the technologies exploiting the solar energy for diverse purposes at the beginning of the 21st century, thanks to awareness of the people regarding the environmental issues. One of these purposes is to supply heating to the buildings from sun. A Double-Flow/Glazed V-corrugated Plate Solar Air Collector (D-F/GVCPSAC) is considered as an effective design that can be used for this purpose.

The principal aim of the present work is to investigate the performance of D-F/GVCPSAC which is intended to be used in an office for space heating during winter in N. Cyprus. The performance investigation has been carried out both numerically and experimentally.

The office space that is intended to be served by the collector is the Mechanical Engineering Department Chairperson office (MEDC Office). The load of the target office has been evaluated by using the Energy Plus building simulation program as 4546W. The thermal performance of a D-F/GVCPSAC is investigated by developing the governing equations and solving them by Matlab program and concurrently carrying out real time monitoring of the collector under the same environmental conditions. It is aimed to obtain the temperature of each element of the collector, the useful heat output, the thermal efficiency, the number of collector and the corresponding area that is necessary to supply the load, as well as comparing the numerical and experimental results.

It is revealed that, there are minor discrepancies between the simulation and experimental results regarding some parameters, whereas in some others the discrepancies are at significant level. It is found that the nine collectors with 16 m^2 are required to supply the target load for the real case (monitoring) and six collectors with 10 m^2 for simulations.

Keywords: Solar air collector, thermal performance, heating load, experimental test, Energy Plus.

ÖZ

İnsanların çevresel konular karşısındaki farkındalığı, güneş enerjisinin çeşitli amaçlar için kullanılmasına olanak sağlayan teknolojilerin 21. Yüzyılda yaygın bir gelişim göstermesini sağlamıştır. Bu amaçlardan birtanesi binaların ısıtma yükünün güneşten karşılanmasıdır. Çift geçişli, çift camlı ve V katlı hava güneş toplayıcısı (D-F/GVCPSAC) bu amaç için kullanılan etkili bir tasarım olarak öne çıkmaktadır.

Bu çalışmanın amacı Kuzey Kıbrıs'ta kış mevsiminde bir iş yerinin ısıtma yükünün karşılanması için kullanılacak olan D-F/GVCPSAC'nin performansını incelemektir. Bu çalışmada D-F/GVCPSAC'nin performansı sayısal ve deneysel olarak incelenmiştir.

Dikkate alınan iş yeri Doğu Akdeniz Üniversitesi Makine Mühendisliği Bölümü Bölüm Başkanlığı'dır. İş yerinin ısıl yükü Energy Plus yazılımı kullanılarak 4546 W olarak hesaplanmıştır. D-F/GVCPSAC'nin performansı aynı iklimsel şartlar altında ilgili denklemlerin oluşturulması, Matlab yazılımı kullanılarak bu denklemlerin çözülmesi ve aynı zamanda deneysel olarak gerekli ölçümlerin gerçekleştirilmesi ile incelenmiştir. D-F/GVCPSAC'nin her katmanının sıcaklıkları, faydalı ısı çıkışı, ısıl verimi ile ısıl yükü karşılamak için gerekli olan toplayıcı saysısı ve alanının belirlenmesi ile sayısal ve deneysel sonuçların karşılaştırmasının yapılması hedeflenmiştir.

Elde edilen sonuçlarda bazı değişkenlerde sayısal ve deneysel sonuçlar arasında büyük farklar olmadığı fakat bazılarında ise dikkate değer farklar olduğu gözlemlenmiştir. Deneysel sonuçlara göre iş yerinin ısıl yükü dokuz toplayıcı ve

buna karşılık gelen 16 m^2 toplayıcı alanı ile karşılanabilirken, sayısal sonuçlara göre altı toplayıcı ve buna karşılık gelen 10 m^2 toplayıcı alanı gerekmektedir.

Anahtar Kelimeler: Hava güneş toplayıcısı, ısıl performans, ısıl yük, deneysel test, Energy Plus.

To My Family

ACKNOWLEDGMENT

Firstly Thanks to Allah Almighty for awarding me the health and ability to achieve the aims of this work successfully.

I would like to thank everybody who helped me to finish this thesis, starting from my generous supervisor (Assist. Prof. Dr. Murat Özdenefe) for his uninterrupted support and encouragement, furthermore, deeply thanks to my friends.

I am grateful to my parents especially and all my dear family for their encouragement and support my morale during my study.

For a significant organized work that has been seen, my thanks to all the staff at Eastern Mediterranean University.

I wish to express special gratitude to my country; our beloved Libyan people, everybody supported me to get this scholarship chance to continue my postgraduate study.

Lastly, I ask Allah Almighty to prevail the peace all my beloved country Libya.

TABLE OF CONTENTS

LIST OF TABLES

LIST OF FIGURES

LIST OF ABBREVIATIONS

D-F/GVCPSAC   Double-Flow/Glazed V-corrugated Plate Solar Air Collector

EMU   Eastern Mediterranean University

MEDC Office   Mechanical Engineering Department, Chairperson Office

SAC/H   Solar Air Collector/Heater

LIST OF NOMENCLATURE

A_a $[m^2]$ Absorber surface area

A_h $[m^2]$ Collector Area

c_p $[J/kg.K]$ Specific heat of air

D_h $[m]$ Hydraulic diameter

G $[W/m^2]$ Solar irradiance

H $[m]$ Thickness

h $[W/m^2 .K]$ Heat transfer coefficient

k $[W/m .K]$ Thermal conductivity

L $[m]$ Length of Collector

$\dot{m}$ $[kg/s]$ Total mass flow rate of crossed air through the collector

N $[-]$ Number of air flow channels

Nu $[-]$ Nusselt number

Nu'_C $[-]$ The number of collectors

Pr $[-]$ Prandtl number

Q_{tu} $[W]$ Total useful energy gain

Q_{off} $[W]$ Heating load of the office building

$\dot{q}_{u1}$ $[W]$ Useful energy gains from upper channel

q_{u2} $[W]$ Useful energy gains from lower channel

R $[m .K/W]$ Total thermal resistance for back of the collector

Ra $[-]$ Rayleigh number

Re $[-]$ Reynolds number

T $[K]$ Temperature

V_w $[m/s]$ Wind speed

W	[m]	Width of Collector

Greek letters

α	[-]	Absorptivity
τ	[-]	Transmittivity
σ	$[W/m^2. K^4]$	Stefane Boltzmann constant
β	[1/K]	Volumetric thermal expansion coefficient
ε	[-]	Emissivity
ν	$[m^2/s]$	Dynamic viscosity
θ	[°]	Tilt angle
ρ	$[kg/m^3]$	Density of flowing air

Subscripts

A	Ambient
Ap	Absorber plate
bp	Back plate
c	Convection
Ex	Experimentally
f1	Air flowing in upper
f2	Air flowing lower channel
g1	Upper glass cover
g2	Lower glass cover
i & o	Inlet & Outlet
ins	Insulation plate
r	Radiation
s	Sky
Sim	Simulation

Chapter 1

INTRODUCTION

1.1 Background

Renewable energy technologies recently have witnessed a significant progress, mainly due to the global demand for clean energy and frequent fluctuations in fossil fuel prices. In spite of growing global economy, in 2014 the first time since four decades, the global emission levels of CO_2 remained at the same level. The essential reasons are due to the efforts of many international organizations and countries in employment of renewables and taken measures regarding the energy efficiency. One example of these efforts is the attempts carried out by the members in the Organization for Economic Co-operation and Development (OECD) to encourage the renewable energy applications and to improve energy efficiency. This is particularly promising as it is planned to recommend new investments on renewables and energy efficiency in the Conference of the Parties (COP21) in Paris, where the members confirmed to mitigate climate change [1].

Of all alternatives, solar energy is considered one of the most important renewable energy source, especially, if it is used directly to produce thermal energy. Solar thermal systems are mature applications for many purposes such as; processes drying in agriculture sector, distillation, water heating, ventilation and heating of the buildings and facilities. These applications become popular in several countries over the past three decades. For example, in Barbados and Cyprus, approximately 80% -

90% of houses have solar water collectors for domestic hot water heating. Globally, these applications are covering just 1.2% of the heating requirements (water and space heating) of buildings [2].

Some countries have other renewable/sustainable energy sources such as; wind, geothermal, hydroelectric and etc. that is more economical to exploit than solar energy. On the other hand, in some regions solar energy is the most efficient and economic energy source among the other renewable sources to supply space and domestic water heating. One of these regions is N. Cyprus which is the considered location for this study.

1.2 Motivation

KIB-TEK is a local state electricity company in N. Cyprus. The annually published report of this company shows that the electricity consumption during 2015 in N. Cyprus is greatest in the residential sector with 29% of the total consumption. The share of electricity consumption of different sectors is illustrated in Figure 1.1 [3].
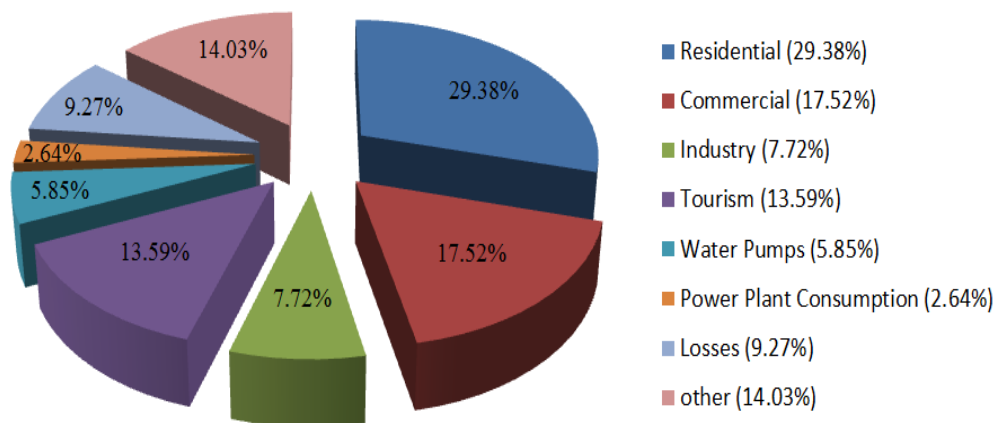
Figure 1.1: Electricity consumption in different sectors in N. Cyprus 2015.

In N. Cyprus space heating accounts 28% of the electricity consumption in the residential sector whereas water heating accounts for 45% of the total and appliances

accounts for 23%. In the residential sector end use share of the electricity consumption for different applications can be seen in Figure 1.2 [4].
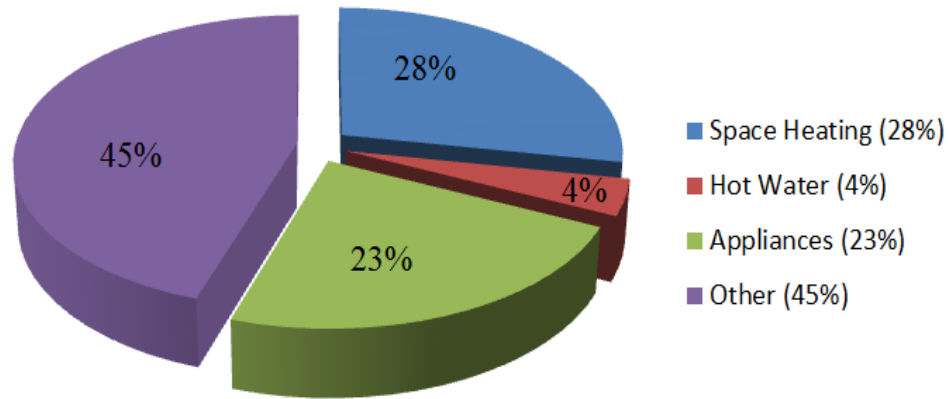
Figure 1.2: North of Cyprus residential sector end use energy consumption [4].

North of Cyprus enjoys more than 300 sunny days throughout a year [5]. Due to its location in the warmest Mediterranean zone, the total of sun hours is the dominant factor which positively influences any solar thermal conversion system in N. Cyprus. Thus, during winter days solar energy can be applied for space heating. Due to these reasons space heating with solar energy is a popular research subject in N. Cyprus, although it does not have widespread real life applications. Some of these researches are mentioned below.

Kahoorzadeh, Shahwarzi, Farjami, and Osivand held a study on a number of buildings in Famagusta, N. Cyprus to investigate the use of passive solar energy for achieving thermal comfort conditions for the building residences[6]. Aldabbagha, Egelioglu, and Al-Khawajah tested two units of single pass SAHs, with different airflow track lengths and wire mesh layers, in order to achieve the most efficient design [7]. A study for designing and manufacturing of a D-F/GVCPSAC has been carried out by Sahebari, Eenesi, and Tamer in N. Cyprus. The group designed and

manufactured the D-F/GVCPSAC for space heating and recommended that tests should be done in order to measure the performance of the manufactured D-F/GVCPSAC [8].

As stated above the space heating and domestic hot water heating is accounting the greatest consumption in the electricity in buildings which is the main motive of this study to consider solar energy exploitation for use in the buildings in N. Cyprus. This work intends to investigate the exploitation of solar energy to cover the space heating demand of the Mechanical Engineering Department Chairperson Office (MEDC Office) located in Eastern Mediterranean University (EMU) in N. Cyprus, Famagusta, by using Double-Flow/Glazed V-corrugated Plate Solar Air Collector (D-F/GVCPSAC).

1.3 Heating Space

N. Cyprus is a potential place for using solar air heaters for space heating; due to its favorable weather thanks to its geographical location. D-F/GVCPSAC is employed to heat the MEDC Office which has floor area of 84 m^2. 3D model of the office is shown in Figure 1.3.
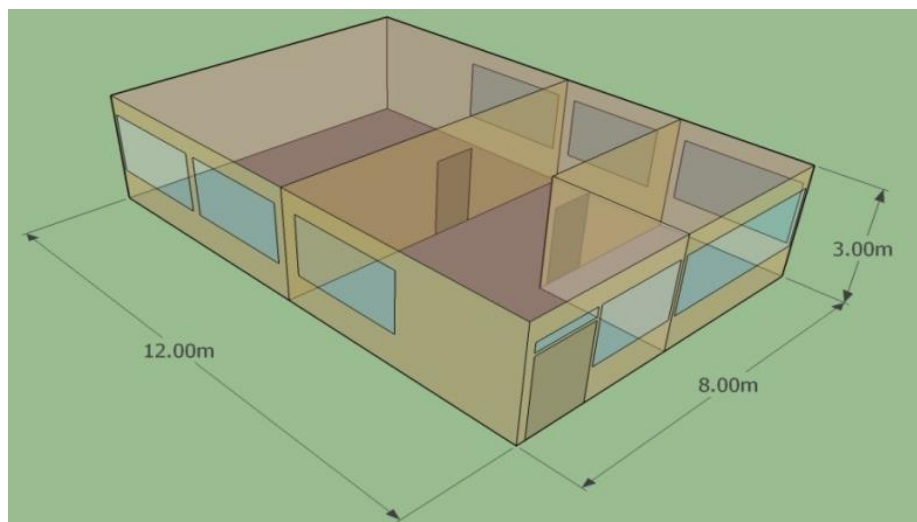
Figure 1.3: 3D model of the space that the solar collector is thought to serve.

1.4 Aims and Objectives

There has been an extensive research on the solar air heaters, various models have been developed for increasing the efficiency of these systems. Although there has been a broad research on this topic particularly in Cyprus, real life applications of these systems to offices for space heating and performance testing has not been carried out extensively.

 In this study, D-F/GVCPSAC that was designed and manufactured by Sahebari, Eenesi, and Tamer [8] will be retrofitted and installed with the ultimate aim of supplying heat to MEDC Office. It is intended to evaluate the required number of solar collectors that will cover the heating demand for a typical winter day for the considered office. It is aimed to investigate the performance of the system experimentally, and compare the results with the estimated values which will result from the solution of the mathematical model of the D-F/GVCPSAC by Matlab.

Energy Plus software will be utilized to estimate the heating load of the office space which is necessary for evaluating the number of Solar Air Collector/ Heater.

1.5 Structure of the Thesis

The existing work consists of six chapters; Introduction, Literature Review, Methodology, Experimental Setup, Results & Discussion and Conclusions. The introduction chapter gives an overview about the renewable energy in general and solar energy in particular. This chapter also focuses on the possibility of solar energy exploitation for space heating in N. Cyprus.

Second chapter provides information about the solar air collectors and the previous studies carried out on them.

The mathematical model and the methodology is presented in chapter 3 which can be summarized as:

- utilization of Energy Plus software to evaluate the heating load of the target office building (MEDC Office).

- utilization of the Matlab program to estimate the thermal efficiency of D-F/GVCPSAC by solving the constructed heat balance equations and evaluate the useful heat output from the collector as well as to find the number of solar collectors that are required to meet the heating load.

The experimental procedure for testing the solar air collector is given in chapter 4.

The results of the simulations and experiments are presented in the results and discussion chapter, chapter 5. Lastly the conclusions are presented in chapter 6.

Chapter 2

LITERATURE REVIEW

2.1 Solar Air Collector/ Heater (SAC/H)

Solar air collectors convert the solar radiation into useful thermal energy, throughout collecting the sun rays that falls on a particular surface area. Their working principle is similar to solar water collectors, except that the working fluid is air [9].

The main components of non- concentration stationary SAC/H are transparent cover (usually glass), insulated air ducts made of wood or metallic materials and absorber plate. Portion of the solar radiation which falls on the glass cover is transmitted through the glass and absorbed by the absorber plate which is usually located above the air duct or ducts depending on the type of SAC/H [10]. Then the air which flows either naturally by density difference (passive SAC) or by a fan (active SAC) exchanges heat with the absorber plate by convection and can be employed for different purposes [11].

Thermal performance of SAC depends on many variables such as dimensions of SAC, absorber type and material, amount of solar radiation, the geometry of the air ducts, the amount of air flow, the type of SAC, etc.

2.1.2 Types of Solar Air Collectors

Solar energy can be converted into thermal energy either by using concentrated or non-concentrated stationary solar collectors, or flat plate collectors (FPC) [9].

FPC can be classified by considering two categories. The first category is the flow type across the FPC, and the second category is the air channel design.

First category types are as follows [11]:

- Single flow single pass: This type is the simplest type such that it consists of only one air pass between a transparent cover, and an absorber plate which is made from high conductive material. The frame of the collector can be insulated by different types of materials such as, glass wool, rock wool or wood.

FPC of this type is illustrated in Figure 2.1 and Figure 2.2. In this type of collector, the flowing air is heated by the direct solar radiation and by convection between the flowing air and the absorber plate.
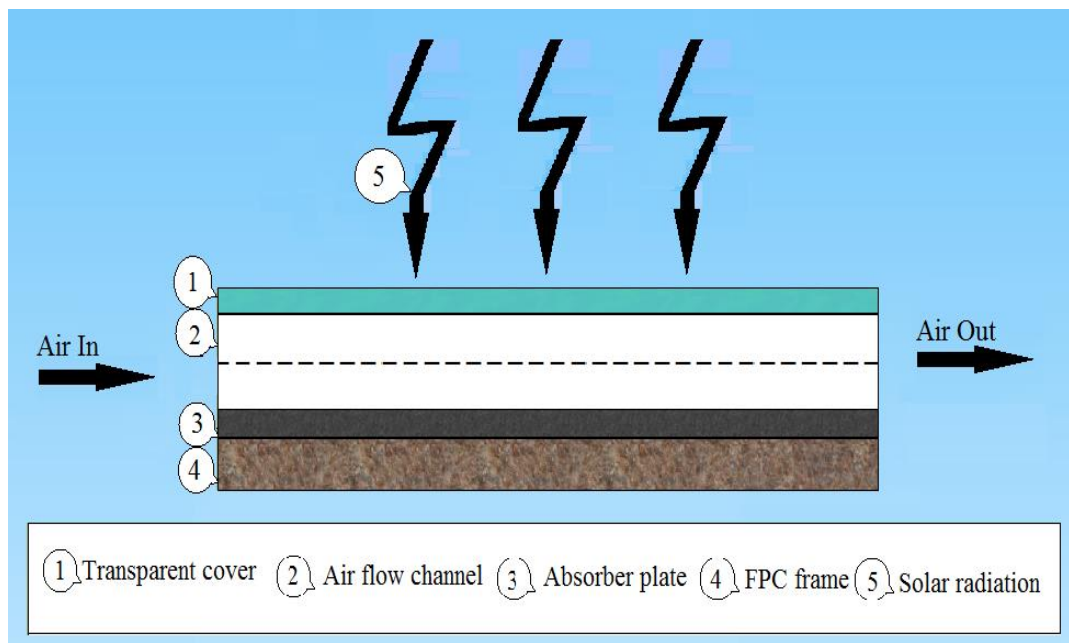
Figure 2.1: Single flow single pass FPC (Redrawn from [11]).
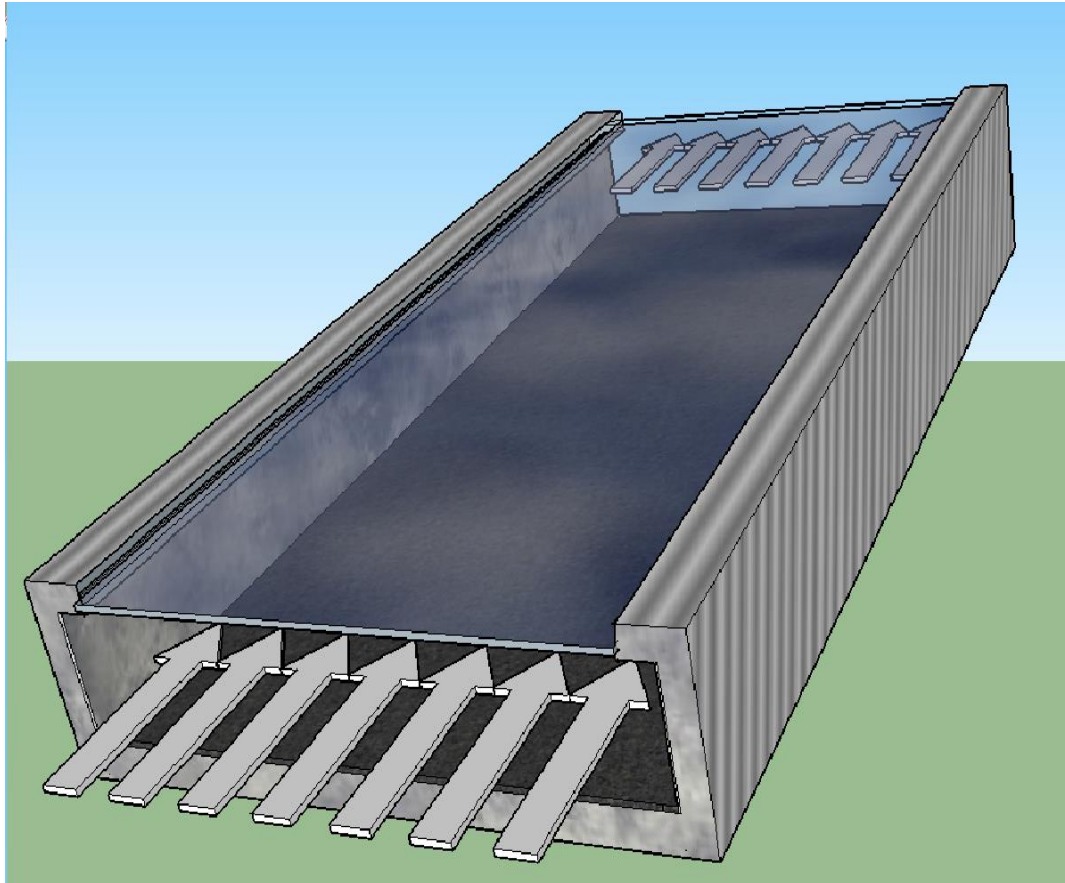
Figure 2.2: 3D Model of Single flow single pass FPC.

- Double flow single pass: Figure 2.3 and Figure 2.4 show the construction of this type, which is similar to the construction of single flow single pass type, except that the flowing air passes across two air channels. In this type a portion of the entering air is heated due to the direct solar radiation and by heat convection between the absorber plate and the flowing air in the upper part of the channel, while the remaining portion of the entering air is heated because of the convection between the flowing air and absorber plate. In this type thermal performance of the FPC heater is higher than the single flow, because the heat exchange area is greater than single flow type.
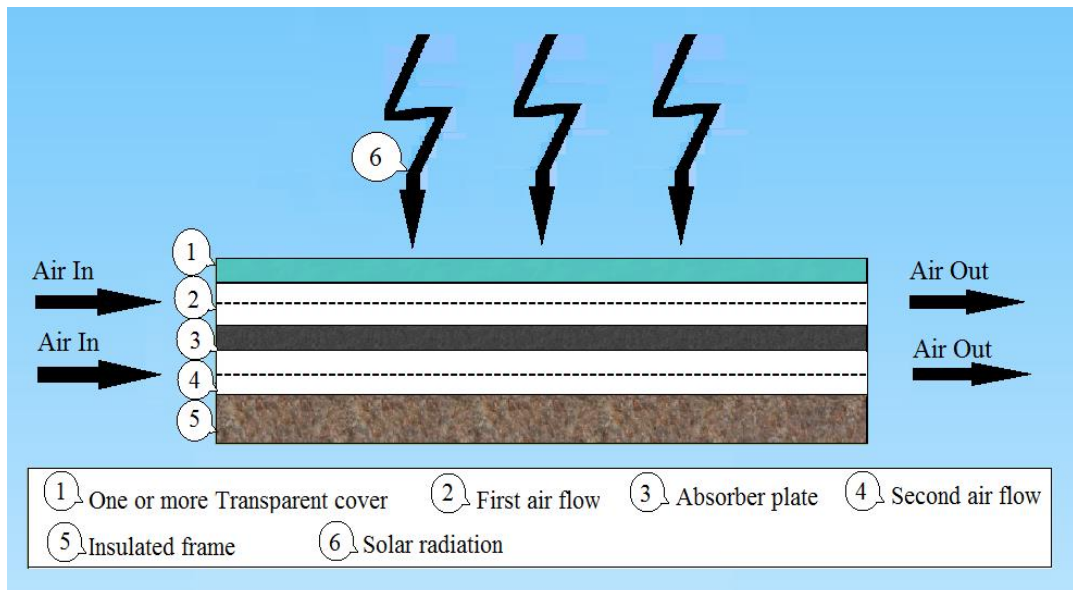
Figure 2.3: Double flow single pass FPC (Redrawn from [11]).
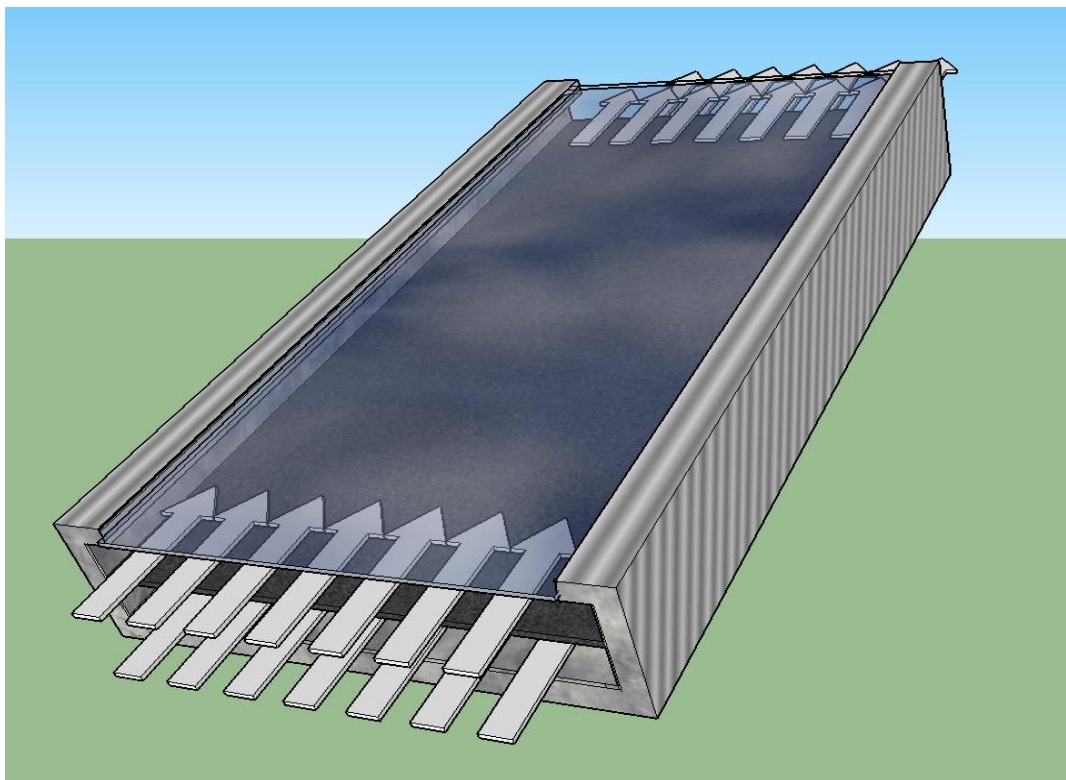
Figure 2.4: 3D Model of Double flow single pass FPC.

- Single flow double pass: In this type the direction of the flowing air changes due to the design of the air channel. This type of collectors can be constructed by two methods Figure 2.5 (a) shows the first construction

10

method in which a transparent plate is placed between the upper and the lower air channels.
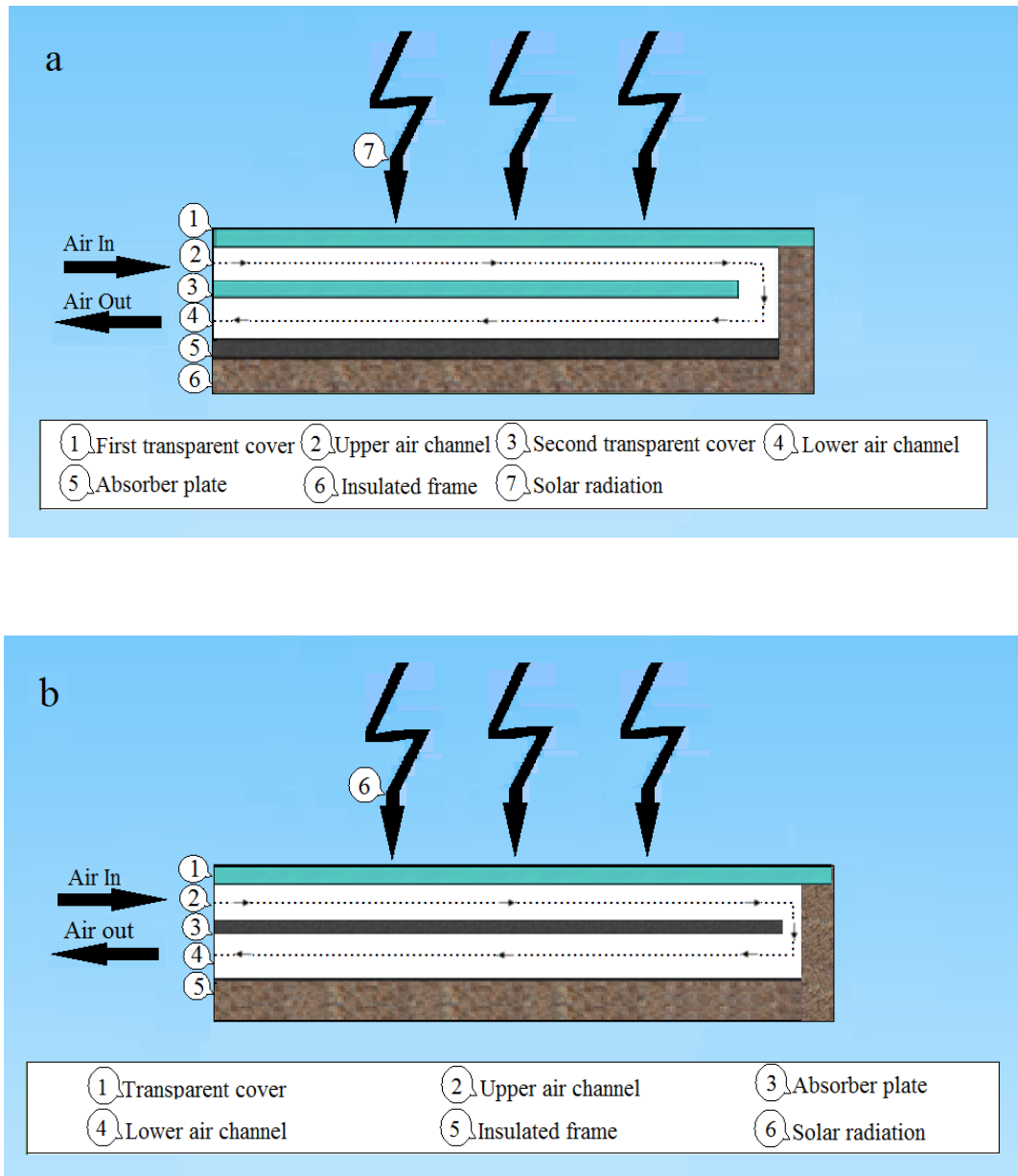
Figure 2.5: a: First method constructed double flow single pass FPC, b: second method constructed double flow single pass FPC (Redrawn from [11]).

- In this construction method, the flowing air in both channels is heated by direct solar radiation and heat convection. The second construction method is shown in Figure 2.5 (b), the absorber plate is placed between the air channels. In this method the flowing air in the upper channel is heated due to direct solar

radiation and convection that occurs between the absorber plate and the flowing air, whereas the flowing air in the lower channel is heated due to convection only. In both construction methods the heat gain of the flowing air is higher than the first two types.

- Single flow recycled double pass: Figure 2.6 shows the construction of this type. The recycled heated air is mixed with entering cold air in this type of collector. Thus, the entering cold air gains heat due to direct solar radiation, convection between the air and the absorber plate and due to the mixing of the recycled heated air.
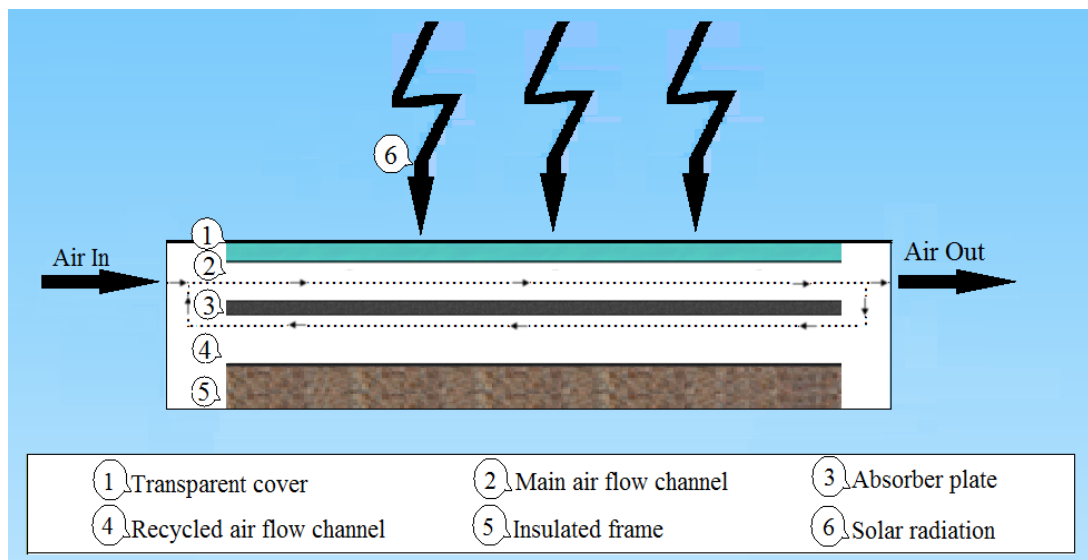
Figure 2.6: Single flow recycled double pass FPC (Redrawn from [11]).

Second category can be classification is based on the design of the air channel and can be divided into; flat plate, porous media and extended surface assisted types. The focus of these designs is to enhance the thermal performance of the collector by varying the parameters which enhance the heat convection. The lending of these parameters is the nature of the flow i.e. turbulent or laminar. The turbulent flows

make heat exchange by convection greater than that of laminar flow because of the mixing vortices which occurring in turbulent flow.

The Solar Collector employed in this study is D-F/GVCPSAC illustrated in Figure 2.7. Two flat glasses cover a v-corrugated absorber plate, shaped as a row of equilateral triangles, which form the upper and the lower flow channels of the incoming air [12].
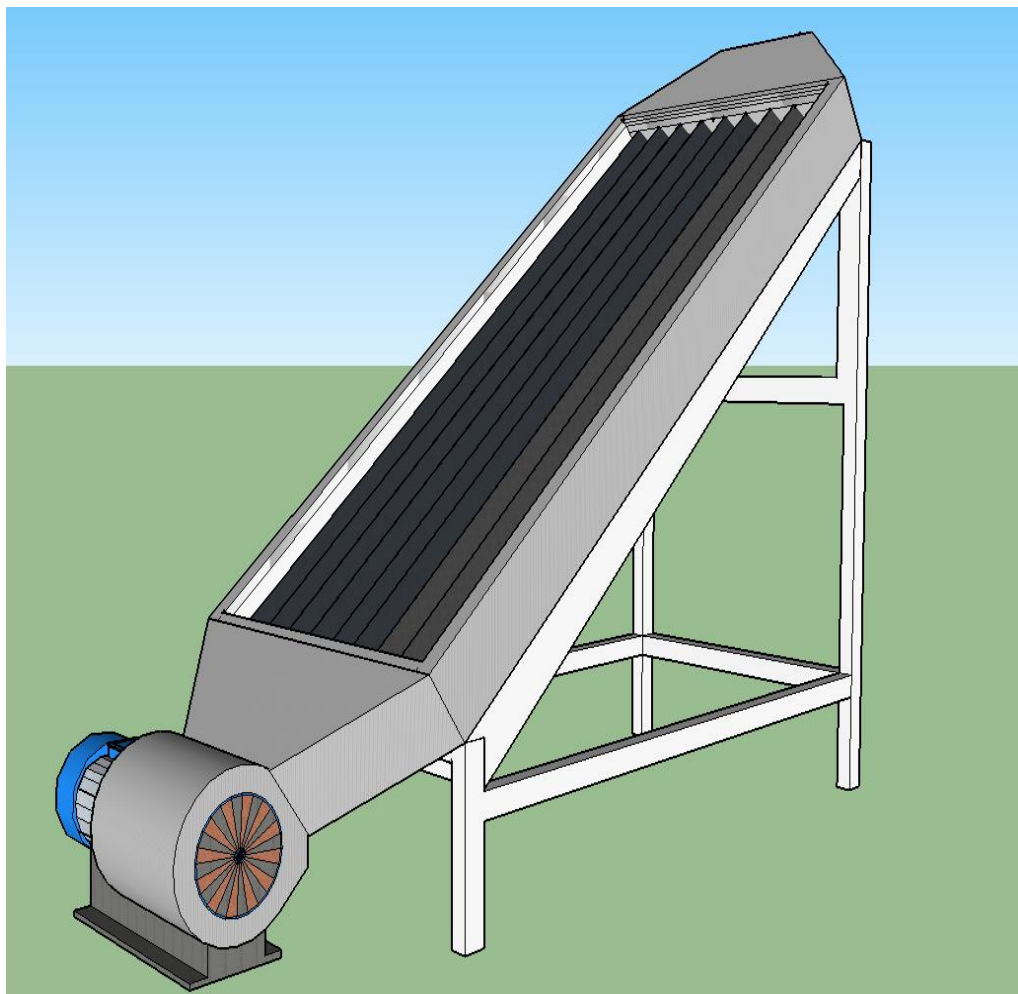
Figure 2.7: 3D Model of D-F/GVCPSAC.

Improvement of the thermal performance of a solar air collector by using a V-corrugated absorber plate is considered as one of the most efficient methods. The main cause of the improvement is the increase of the absorber plate area (A) and also

the enhancement of the convection heat transfer coefficient (h) due to the corrugated shape, which obviously affects positively the radiative characteristics of the absorber plate [13].

2.2 Previous Studies on Solar Air Heaters

Current and future energy crises, enforces the researchers for finding alternative renewable energy sources. Solar energy which is a promising source is now used in many applications. Solar Air Collectors (SACs) is applied widely for heating and drying for low temperature applications [14]. Also SAC are used especially in summer time in building sector for ventilation purposes, to produce an air flow current inside the building envelop [15].

Passive heating and cooling is a solution for reducing energy crises and solar energy is an efficient way that can be used directly for passive heating of buildings [16]. However, passive heating still is insufficient to preserve the thermal comfortability in regions where there is not enough solar radiation during sun shining time [17]. Therefore, the thermal performance of solar passive heating with storage equipment has to be enhanced. Schmidt, Mangold, and Müller-Steinhagen presented the results of a central solar heating station with heating storage system that preserved 10-20% of the total seasonal space heating required [18].

It can be concluded that solar thermal energy is a promising renewable energy source for space heating, but still it is insufficient to be used alone especially in regions with poor solar radiation.

Many factors that affect the thermal performance of flat plate solar air heaters are studied. The increase in the airflow rate increased the efficiency of a vertical flat

double-pass solar air heater with a recycle airflow channel [19]. Ben-Amara, Houcine, Guizani and Maalej investigated the effect of solar radiation, airflow, ambient conditions and humidity of flowing air inside the collector which used for water desalination [20].

Turbulent flow enhances the convection heat transfer and rough surfaces can increase the turbulence of the flowing air inside the collector. Karwa and Chauhan investigated a 60º V shape roughness element attached to the air channel. The authors found that the roughness increased the efficiency of the collector for airflow rate of 0.04 kg /s per m^2[21].

Alta, Bilgili, Ertekin, & Yaldiz investigated the effect of airflow rates of 25, 50 and 100 m^3 per m^2 hour, and collector title angles of 0º, 15º and 30º on the efficiency of flat plate solar air heater. They found that efficiency of the collector improved by the increase of the airflow rate, while the inlet and outlet temperature difference of the collector decreases if the title angle held constant [22].

However, Nowzaria, Aldabbagh, and Mirzaei found in their experiments which were carried out in Famagusta, N. Cyprus that the difference between the outlet and inlet temperatures of solar collectors decreases with the increase of the airflow rate [10].

Joudi & Farhan used a six V-corrugated single glass collector plates connected in parallel for winter heating of a greenhouse. The plates provided 84% of the required daily heating demand to keep the greenhouse inside temperature at 18ºC with an airflow rate of 0.012 kg/s.m^2 [23].

Bashria Abdrub Alrasoul Abdallah Yousef and Adam tested the effect of the depth of the air channel, the length and the airflow rate on the performance of a single and double flow mode V-groove solar air collector. It is found that the double flow is more efficient by 4-5% than a single flow if a porous media is used [24].

The most important parameters that affect air solar collectors are the design of the absorber plate and the shape of the airflow channel. This is stated by Karim, Amin, and Almunasif who developed mathematical models for a single and double v-groove solar collectors to compare their efficiencies. The authors also stated that, heat loss affect the performance of the collector. The author's simulation results revealed that the double flow has higher efficiency by 56% at flow rate of 0.06 kg/m^2s [25].

It can be concluded from the literature that, solar air collectors can be used for space heating as standalone heating system, if the weather conditions are suitable and the system is properly designed.

Chapter 3

MATHEMATICAL MODELING

3.1 Introduction

The software development has been witnessed a considerable advance in recent years, and this enhanced the employment of softwares in many engineering applications and contributed to achieve swift solutions to almost any engineering problems. Thus, today numerous simulation softwares are available to serve the designers to provide accurate predictions by simulating reality with a small percentage of error. In this regard, there are powerful simulation programs such as Energy Plus and Matlab that are ready to be used to achieve the goals of the present study. These two programs are used extensively in this work.

This chapter describes the methodology and mathematical modeling that is followed in this study. The load evaluation of the office space has been carried out and mathematical model of the considered solar collector is generated. The load of the office space is evaluated by Energy Plus software whereas the mathematical model of the collector is solved for associated temperatures and useful heat output via Matlab program. The evaluated useful heat output from the collector is used together with the load of the office space to find the number of solar collectors that are necessary to cover the heating demand of the space during a typical winter day. The solar collector that has been modeled is a real collector produced previously in the Mechanical Engineering Department.

The collector is retrofitted and prepared for experimental test. Temperature measurements of the collector elements together with the environmental variables (solar radiation, wind speed, etc.) have been taken and used to evaluate the useful heat output from the collector. The outputs of the Matlab code have been compared with the experimental results to reveal the difference between the actual and model performance of the collector. The Methodology which has been followed is generated as a flow chart and is given in Figure 3.1.
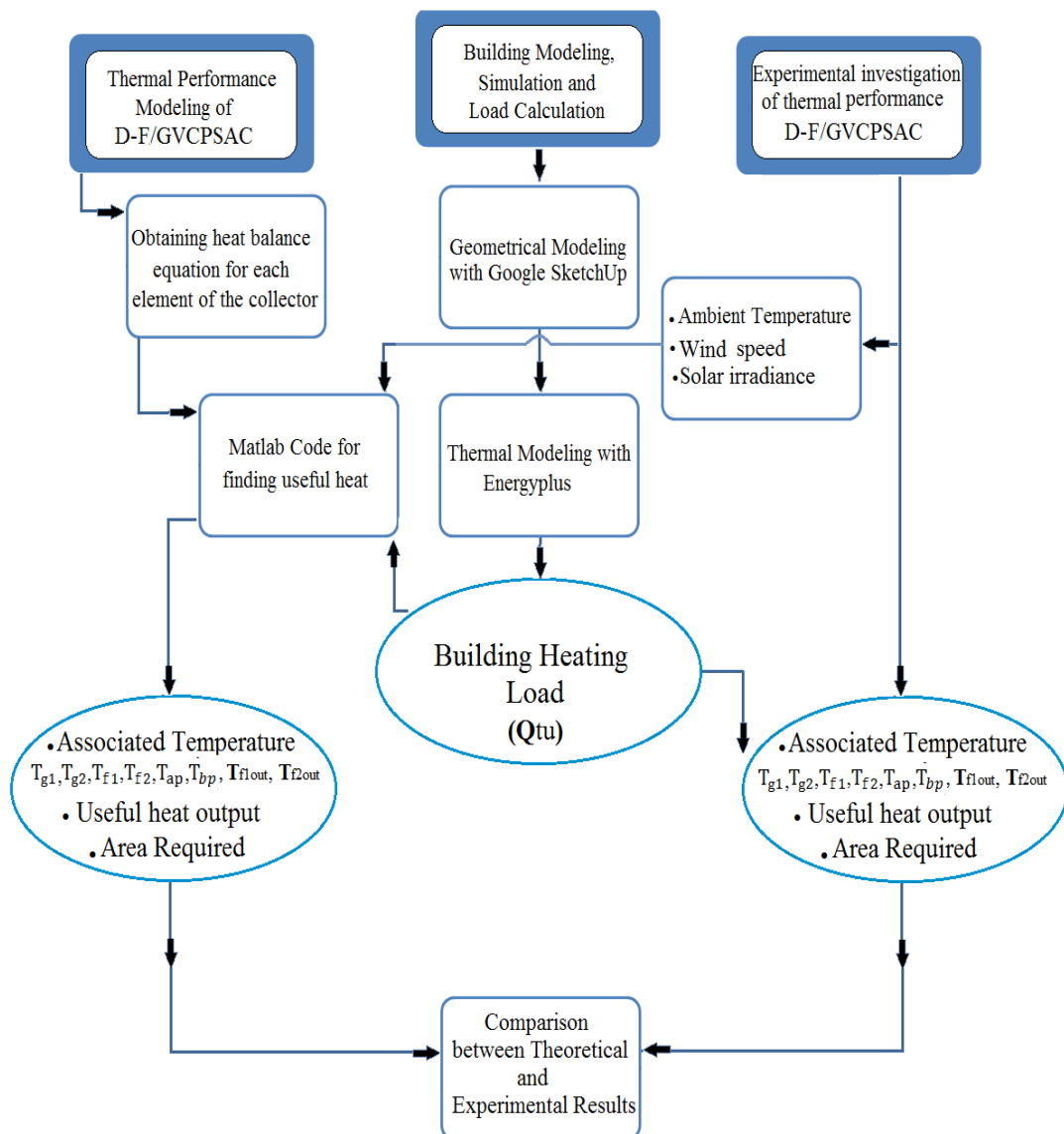
Figure 3.1: Flowchart of Methodology.

3.2 Building Energy Simulation and Load Calculation

The first purpose in this chapter is to evaluate the heating load of the considered office building. The load evaluation is done by utilizing the Energy Plus program (Version 8.5), which is able to determine the amount of the heating load for each particular zone within the building and able to carry out energy simulation.

3.2.1 Energy Plus

Energy plus software is a dynamic energy and load calculation tool which is used to evaluate the energy use, heating and cooling loads of the buildings. It has been developed by the US Department of Energy [26] to be a complete simulation tool that could be employed for several applications related to energy flows in the buildings.

Energy Plus software has been designed as a simulation engine and the installed package comes with some utilities for running process, for constructing input files and for generating 3D building models. These utilities are EP-launch, IDF editor and the Open Studio plugin in Google SketchUp that has been developed by Peter Ellis of the National Renewable Energy Labs to provide fundamental design tools for geometrical modeling for Energy Plus [27], [28]. Energy Plus is made up from various modules which every module is designed for modeling and simulating a particular application. The internal modules of Energy Plus can be seen in Figure 3.2 [29].

In addition, there are other files and auxiliary programs that can be fed to and embedded into Energy Plus such as Weather Data Files, example files generator and 3D Ground Heat Transfer Tool to enable a proper building simulation. Every building simulation program has to employ a weather file that characterizes local

weather conditions in order to carry out load calculation and energy simulation. In this work, unfortunately, the weather data file for Famagusta is unavailable, so for that, the weather data for Larnaca is chosen as the nearest location, which is available.
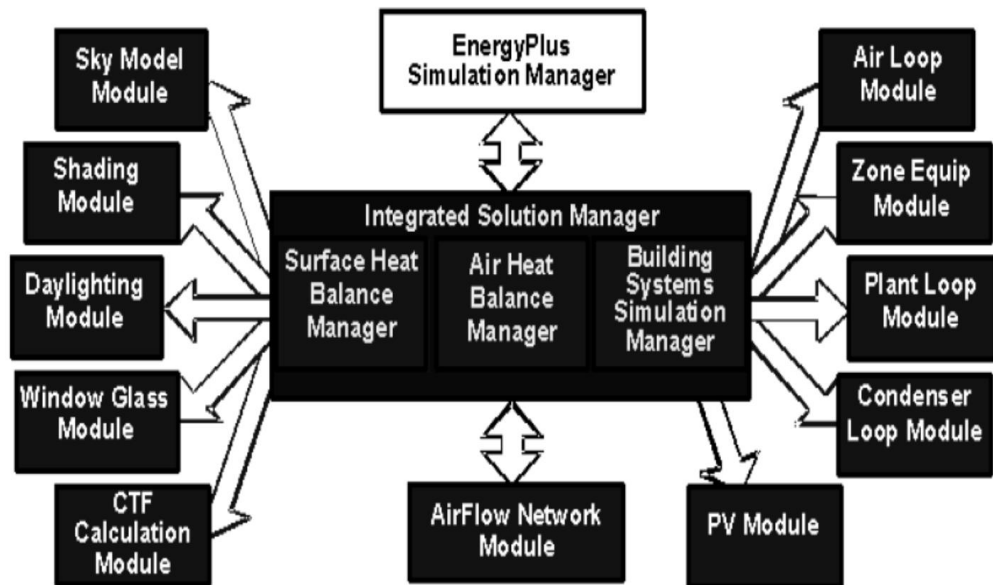
Figure 3.2: The internal modules of Energy Plus [29].

Energy Plus software follows ASHRE standards and heat balance equations for evaluating space heating and cooling loads. The software is designed to solve the heat balance equations for each element of the building (roof, ceiling, walls, etc.) [29].

The software counts for transient heat conduction through building elements by employing conduction transfer functions (CTF). CTF converts the transient heat conduction equations for the outside and inside face temperatures, into simple set of linear equations.

The basic formula of (CTF) solution can be defined by the equations (3.1), (3.2) [29]:

For the internal heat flux

$$q''_{ki}(t) = Z_o T_{i,t} - \sum_{j=1}^{nz} Z_j T_{i,t-j\delta} + Y_o T_{o,t} + \sum_{j=1}^{nz} Y_j T_{o,t-j\delta} + \sum_{j=1}^{nq} \Phi_j q''_{ki,t-j\delta} \qquad 3.1$$

For the external heat flux

$$q''_{ko}(t) = -Y_o T_{i,t} - \sum_{j=1}^{nz} Y_j T_{i,t-j\delta} + X_o T_{o,t} + \sum_{j=1}^{nz} X_j T_{o,t-j\delta} + \sum_{j=1}^{nq} \Phi_j q''_{ko,t-j\delta} \qquad 3.2$$

Where,

q''_{ki} : Conduction heat flux on inside face,

q''_{ko}: Conduction heat flux on outside face,

T_i: Inside face temperature,

T_o: Outside face temperature,

 i : signifies the inside of the building element,

0: signifies the outside of the building element,

t: represents the current time step,

X_j : Outside CTF coefficient, j= 0,1,…nz,

Z_j : Inside CTF coefficient, j= 0,1,…nz.

Y_j : Cross CTF coefficient, j= 0,1,…nz.

3.2.2 The Office Modeling

As a first step, it is aimed to examine the construction materials, lighting, and the electrical capacity of the appliances (for internal loads). The dimensions of the office space are required as well in order to generate the 3D model of the office space.

Table 3.1 and Table 3.2 show the data that is collected, and Figure 3.3 illustrates the floor plan of the office building. Accordingly, a 3D office model is generated by Google Sketchup as shown in Figure 3.4.

The 3D model of the office space is exported to Energy Plus and the necessary data which is given in Table 3.1 and Table 3.2 together with the local weather data (for

Larnaca) in terms of weather data file are inputted to Energy Plus. Subsequently, a simulation run is carried out for the modeled space in order to evaluate the heating load.

Table 3.1: The requisite Input data for Energy Plus IDF Editor

Heating setpoint temperature	20°C
Lighting	7 Fluorescent ,58W each: (7x58=406W)
Occupants	3 persons
Electric Equipment	(Refrigerator, 3 Laptop Computers, 2 Desktop Computers, Printer) ≈1200W
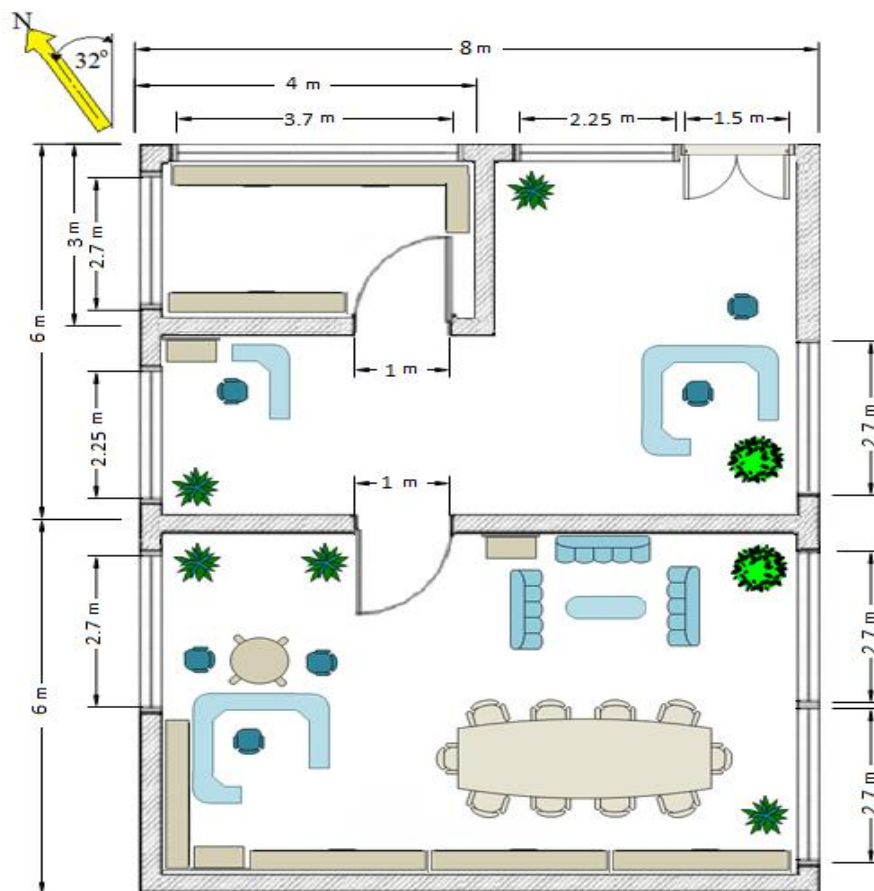
Figure 3.3: Floor plan of the target office building (MEDC Office).

Table 3.2: Office thermal sources properties [30].

No	Item type	Material (Thickness)	Thermal conductivity k(W/m.K)
1	Exterior & Interior walls	Bricks thickness (250 mm)	0.4
		2 cement plaster layers (25 mm each)	1.4
2	Interior Floor or Interior Ceiling(Matching surface)	Marble(20 mm)	2.9
		Screed(15 mm)	1.4
		Reinforced concrete(200 mm)	2.1
		cement plaster (25 mm)	1.4
3	Exterior Floor	Marble(20 mm)	2.9
		Screed(15 mm)	1.4
		Reinforced concrete(200 mm)	2.1
4	Exterior Roof	Screed(15 mm)	1.4
		Reinforced concrete(200 mm)	2.1
		cement plaster (25 mm)	1.4
5	Exterior & Interior Window	Single glass (3 mm)	3.23646 U-Factor
6	Exterior Door	Hardwood (25 mm)	0.167
7	Interior Door	Wood(25 mm)	0.15
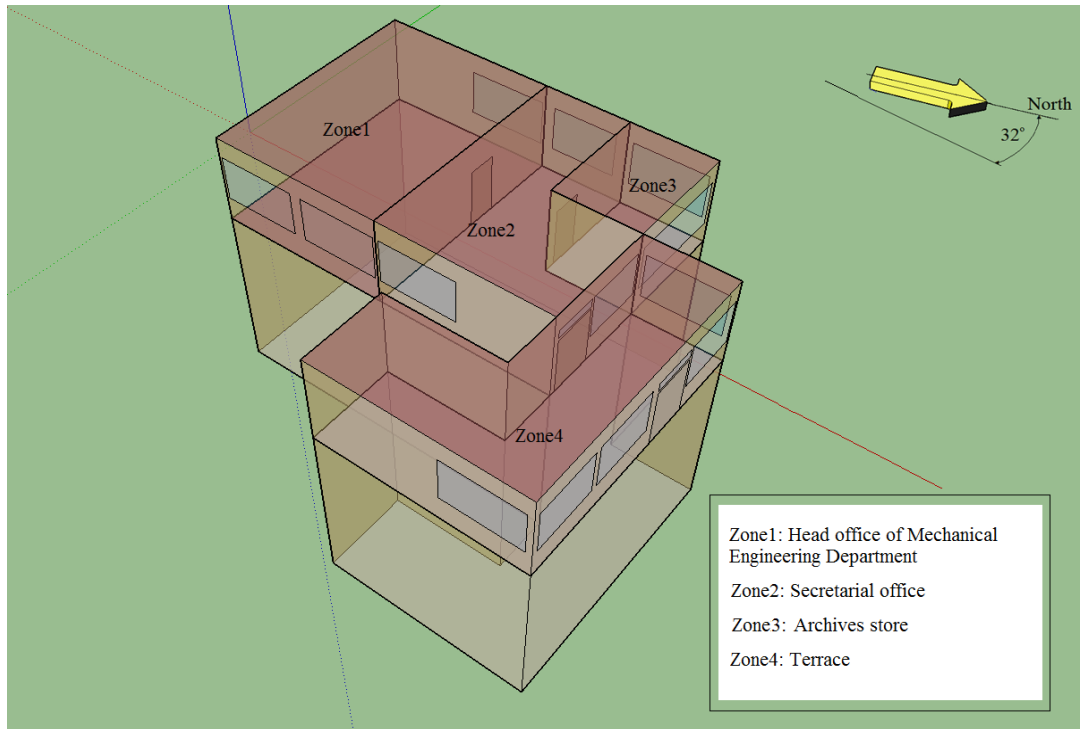
Figure 3.4: 3D model of the MEDC Office located in EMU at N. Cyprus.

3.3 Mathematical Model of a (D-F/GVCPSAC).

It is intended in this work to estimate the number of collectors that is required to supply the amount of heat required to cover the load of the particular space (MEDC Office) for a typical winter day. In order to do that useful heat output from the collector is to be evaluated. Useful heat can be evaluated by multiplying the mass flow rate of the flowing air with the specific heat of the air and inlet & outlet air temperature difference. Specific heat of air and the mass flow rate is known. However the outlet air temperature of the collector should be evaluated. This requires the estimation of temperatures of each constituent (e.g. glass, absorber plate, air layer etc.) of the solar collector. The temperatures of the each element of the collector are evaluated by using the general energy balance. Energy balance for each component is written separately and resulting algebraic equations are used to construct a matrix and are solved simultaneously.

24

The Figure 3.5 and Figure 3.6 illustrate the heat transfer coefficients for each element of D-F/GVCPSAC and the components of it. The components are two flat transparent covers, a V-corrugated absorbing plate, a flat absorbing plate, and the back elements of the collector that are assembled to be under the flat absorbing plate (these are: insulation, wooden box, external cover protect of the wooden box). Table 3.3 shows the features of each component of the collector.

In order to develop the mathematical model for the D-F/GVCPSAC some assumptions have been done. These assumptions are [31], [32]:

- Thermal performance is considered to be steady state.

- Heat flow through the back components (Flat absorber plate, Insulated plate, bottom side of the wooden box, external cover) is considered to be one dimensional.

- The thermal inertia of each collector component is neglected.

- Both of the air channels are free of leakage.

- During operation, temperature values of each collector component are uniform.

- The sky can be considered as a blackbody for long wavelength radiation at an equivalent sky temperature.

- Heat loss through the front and back side of the collector is to the same ambient temperature.

- The shading generated by the V-corrugated absorber, dirt and dust on the collector are considered to be negligible.

- The air temperature varies in the heat flux direction.

Table 3.3: Descriptions of each component of a D-F/GVCPSAC[8].

Component	Material & Dimensions
External cover of D-F/GVCPSAC	Galvanized Steel out layer [200 cm *100 cm * 20 cm]
Two Transparent Covers	Glass [For each piece 194 cm * 94 cm with thickness 0.4 cm]
V- corrugated Absorber	Galvanized Steel dyed in black [V- (60°) corrugated with thickness 0.2 cm]
Flat Absorber plate	Galvanized Steel [97 cm * 96 cm with thickness 0.2 cm]
Wooden box	Balsa wood shaped as U letter[200cm*100cm, Height of each side 20cm with thickness 4cm]
Insulation	polystyrene layers, [for each side :15cm*197cm, with thickness 2cm] [for the Back: 197 cm *97 cm with thickness 2 cm]
Stand	Steel [tilted the Collector with 45°]
Fan	[60-220V with Controller Tool on the fan speed]
Inlet and Outlet Air Duct	Galvanized Steel shaped as V letter as shown in Figure 3.6
Fan Stand	Balsa Wood [0.28 m^2]
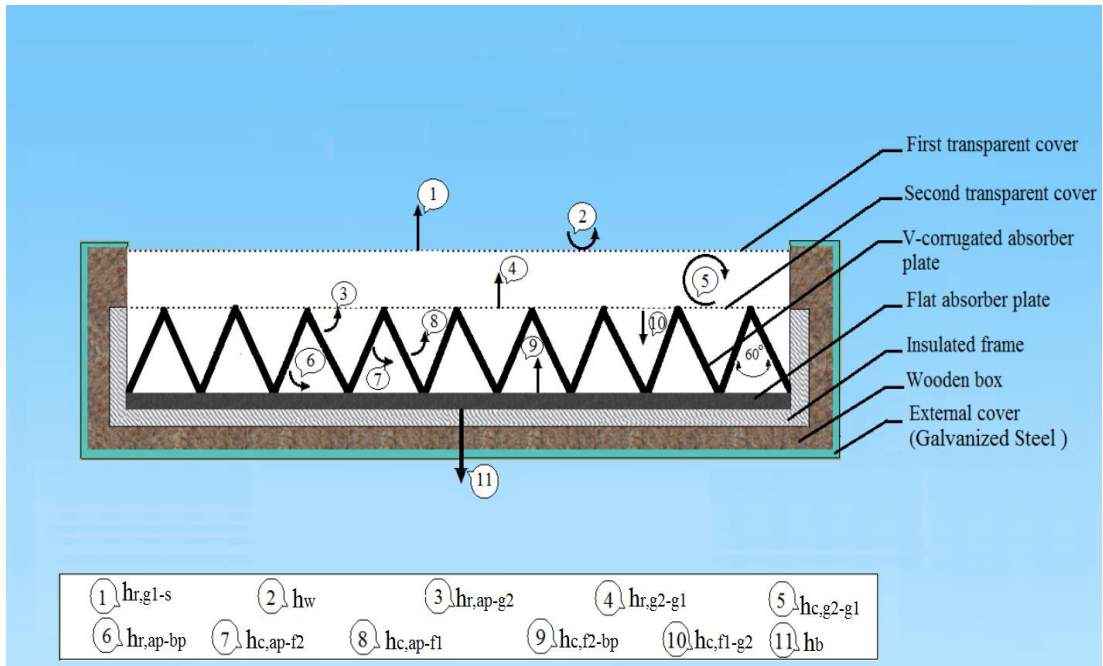
Figure 3.5 : heat transfer coefficients between the elements of D-F/GVCPSAC.

① $h_{r,g1-s}$		② h_w		③ $h_{r,ap-g2}$		④ $h_{r,g2-g1}$		⑤ $h_{c,g2-g1}$		
⑥ $h_{r,ap-bp}$	⑦ $h_{c,ap-f2}$		⑧ $h_{c,ap-f1}$		⑨ $h_{c,f2-bp}$		⑩ $h_{c,f1-g2}$		⑪ h_b	

L: Length of heater (m)   W: Width of heater (m)   H1: Thickness of the air layer between glass plates (m)

H2: Height of the Air Duct (m)   H3: Thickness Of The Insulated plates (m)
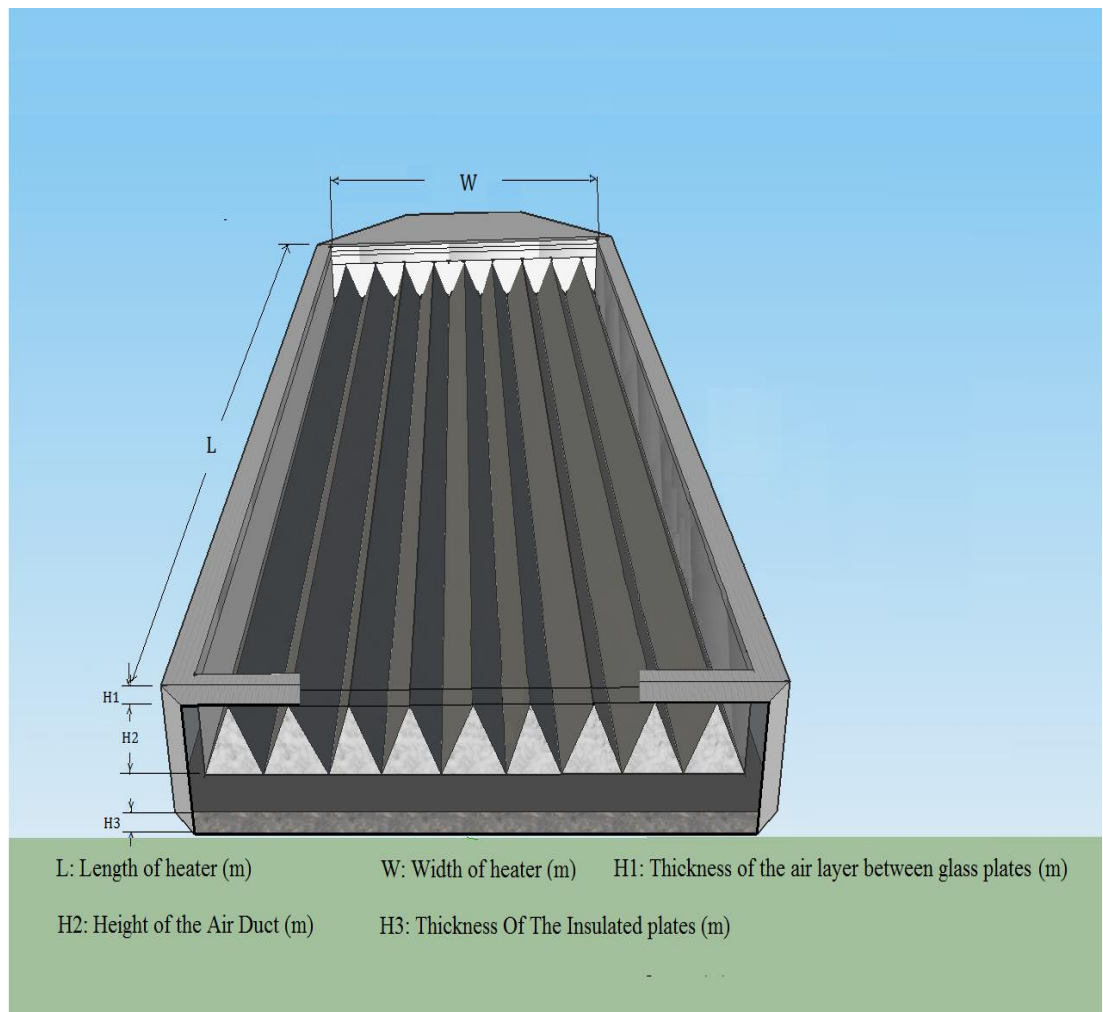
Figure 3.6 : D-F/GVCPSAC schematic diagram.

3.3.1 Energy Balance Equations

The equations of energy balance are constructed based on the thermal resistance network which is shown in Figure 3.7.
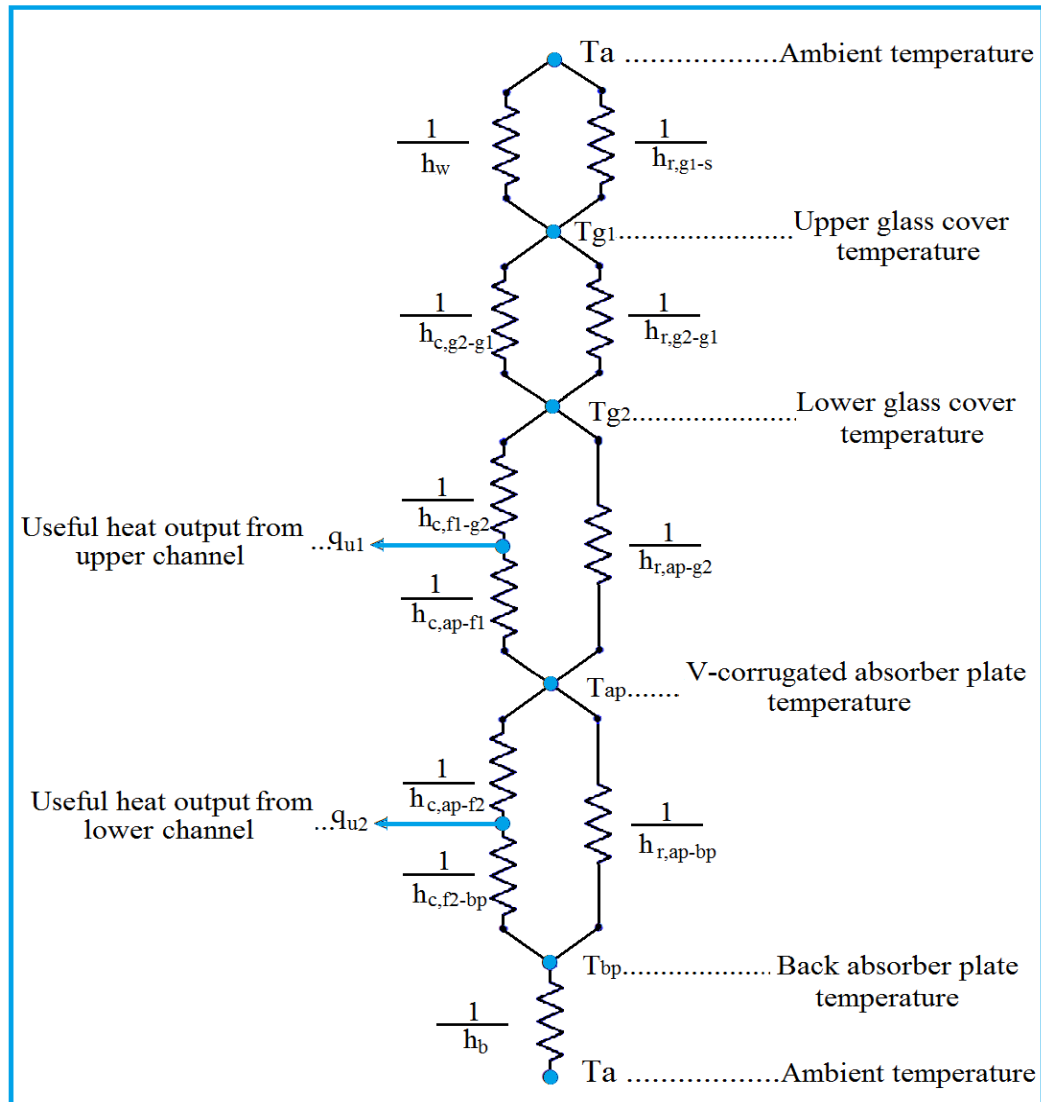
Figure 3.7 : Thermal resistance network for D-F/GVCPSAC.

The energy balances for the upper glass layer, lower glass layer, air located in the upper channel and air located in the lower channel are written as in equation 3.3 to 3.6 respectively [12]:

$$\alpha_{g1}GA_h + (h_{r,g2-g1} + h_{c,g2-g1})(T_{g2} - T_{g1})A_h = h_w(T_{g1} - T_a)A_h + h_{r,g1-s}(T_{g1} - T_s)A_h \tag{3.3}$$

$$\tau_{g1}\alpha_{g2}GA_h + h_{r,ap-g2}(T_{ap} - T_{g2})A_a + h_{c,f1-g2}(T_{f1} - T_{g2})A_h = (h_{r,g2-g1} +$$

$$h_{c,g2-g1})(T_{g2} - T_{g1})A_h, \tag{3.4}$$

$$h_{c,ap-f1}(T_{ap} - T_{f1})A_a = \dot{q}_{u1} + h_{c,f1-g2}(T_{f1} - T_{g2})A_h, \tag{3.5}$$

$$h_{c,ap-f2}(T_{ap} - T_{f2})A_a = \dot{q}_{u2} + h_{c,f2-bp}(T_{f2} - T_{bp})A_h, \tag{3.6}$$

The air temperatures are considered as the average of the inlet and outlet air temperatures for both channels which are given in Eqs. (3.7.a) and (3.7.b);

$$T_{f1} = (T_{f1i} + T_{f1o})/2, \tag{3.7.a}$$

$$T_{f2} = (T_{f2i} + T_{f2o})/2, \tag{3.7.b}$$

The useful thermal energy output from upper and lower air channels of the collector is obtained from Eqs. (3.8.a) and (3.8.b) respectively;

$$\dot{q}_{u1} = \dot{m}c_p(T_{f1o} - T_{f1i})/2 \tag{3.8.a}$$

$$\dot{q}_{u2} = \dot{m}c_p(T_{f2o} - T_{f2i})/2 \tag{3.8.b}$$

The total useful thermal energy output (Q_{tu}) and the thermal efficiency of the collector (η_{TH}) are expressed by Eqs. (3.9) and (3.10):

$$\dot{Q}_{tu} = \dot{q}_{u1} + \dot{q}_{u2} \tag{3.9.a}$$

$$\eta_{TH} = \frac{\dot{Q}_{tu}}{GA_h} \times 100 \tag{3.9.b}$$

The number of collectors (Nu'_C) and the total area required (A_{total}) to meet the heating load of the office building can be obtained as:

$$Nu'_C = \frac{Q_{off}}{Q_{tu}} \tag{3.10.a}$$

$$A_{total} = A_h * Nu'_C \tag{3.10.b}$$

The energy balance for the V-corrugated and flat absorber plate are given in the Eqs. (3.11) and (3.12) respectively [12],[31];

$$\tau_{g1}\tau_{g2}\alpha_{ap}GA_a = h_{r,ap-g2}(T_{ap} - T_{g2})A_a + h_{c,ap-f1}(T_{ap} - T_{f1})A_a + h_{c,ap-f2}(T_{ap} - $$

$$T_{f2})A_a + h_{r,pa-bp}(T_{ap} - T_{bp})A_a \qquad 3.11$$

$$h_{r,ap-bp}(T_{ap} - T_{bp}) + h_{c,f2-bp}(T_{f2} - T_{bp}) = h_b(T_{bp} - T_a) \qquad 3.12$$

By simple mathematical manipulation of the previous energy balance equations, the temperatures of each element of the collector can be expressed in below forms which are given in Equation (3.13) to (3.16);

Based on Eq. (3.3), the temperature of the upper glass layer is obtained as,

$$T_{g1} = \frac{(\alpha_{g1}G + (h_{r,g2-g1} + h_{c,g2-g1})T_{g2} + h_wT_a + h_{r,g1-s}T_s)}{(h_{r,g2-g1} + h_{c,g2-g1} + h_w + h_{r,g1-s})} \qquad 3.13$$

Based on Eq. (3.4), the temperature of the lower glass layer is obtained as in Eq. (3.14),

$$T_{g2} = \frac{\tau_{g1}\alpha_{g2}GA_h + h_{r,ap-g2}T_{ap}A_a + h_{c,f1-g2}T_{f1}A_h + (h_{r,g2-g1} + h_{c,g2-g1})T_{g1}A_h}{h_{r,ap-g2}A_a + (h_{c,f1-g2} + h_{r,g2-g1} + h_{c,g2-g1})A_h} \qquad 3.14$$

Based on Eq. (3.5), temperature of air flowing in upper channel is obtained as in Eq. (3.15),

$$T_{f1} = \frac{h_{c,ap-f1}T_{ap}A_a + \dot{m}c_pT_a + h_{c,f1-g2}T_{g2}A_h}{h_{c,ap-f1}A_a + \dot{m}c_p + h_{c,f1-g2}A_h} \qquad 3.15$$

Based on Eq. (3.6), temperature of air flowing in lower channel is obtained as in Eq. (3.16),

$$T_{f2} = \frac{(h_{c,ap-f2}T_{ap}A_a + \dot{m}c_pT_a + h_{c,f2-bp}T_{bp}A_h)}{(h_{c,ap-f2}A_a + \dot{m}c_p + h_{c,f2-bp}A_h)} \qquad 3.16$$

Based on Eq. (3.11), temperature of the V-corrugated absorber plate is obtained as in

Eq. (3.17),

$$T_{ap} = \frac{(\tau_{g1}\tau_{g2}\alpha_{ap}GA_h + h_{r,ap-g2}T_{g2}A_a + h_{c,ap-f1}T_{f1}A_a + h_{c,ap-f2}T_{f2}A_a + h_{r,ap-bp}T_{bp}A_a)}{(h_{r,ap-g2} + h_{c,ap-f1} + h_{c,ap-f2} + h_{r,ap-bp})A_a} \qquad 3.17$$

Based on Eq. (3.12), temperature of the back absorber plate is obtained as in Eq. (3.18),

$$T_{bp} = \frac{h_b\,T_a + h_{r,ap-bp}T_{ap} + h_{c,f2-bp}T_{f2}}{h_b + h_{r,ap-bp} + h_{c,f2-bp}} \qquad 3.18$$

Heat balance equations (3.3),(3.4),(3.5),(3.6),(3.11) and (3.12) can be expressed as a 6 x 6 matrix notation, as (see figure 3.8):

$$[A] * [T] = [B] \qquad 3.19$$

[A] is a non-homogeneous matrix which is made up from the coefficients of the temperatures of the elements (glass 1, glass 2, flowing air, etc.) of the collector. [T] is the column matrix which is made up from the temperature values of the elements of the collector. [B] is also a column matrix which is formulated by using the heat transfer coefficients, environmental parameters and thermophysical properties of the elements. The governing equations for the column vector [B] have been derived and are given in the subsequent section.

$$
\begin{bmatrix}
(h_{r,g2-g1}+h_{c,g2-g1}+h_w+h_{r,g1-s}) & -(h_{r,g2-g1}+h_{c,g2-g1}) & 0 & 0 & 0 & 0 \\
-(h_{r,g2-g1}+h_{c,g2-g1})A_h & (h_{r,ap-g2}A_a+(h_{c,f1-g2}+h_{r,g2-g1}+h_{c,g2-g1})A_h) & -(h_{c,f1-g2})A_h & -(h_{r,ap-g2}\,A_a) & 0 & 0 \\
0 & -(h_{c,f1-g2})A_h & h_{c,ap-f1}A_a+\dot{m}c_p+h_{c,f1-g2}A_h & -(h_{c,ap-f1})A_a & 0 & 0 \\
0 & -(h_{r,ap-g2})A_a & -(h_{c,ap-f1})A_a & (h_{r,ap-g2}+h_{c,ap-f1}+h_{c,ap-f2}+h_{r,ap-bp})A_a & -(h_{c,ap-f2})A_a & -(h_{r,ap-bp}A_a) \\
0 & 0 & 0 & -(h_{c,ap-f2})A_a & (h_{c,ap-f2}A_a+\dot{m}c_p+h_{c,f2-bp}A_h) & -(h_{c,f2-bp}\,A_h) \\
0 & 0 & 0 & -(h_{r,ap-bp}) & -(h_{c,f2-bp}) & (h_b+h_{r,ap-bp}+h_{c,f2-bp})
\end{bmatrix}
*
\begin{bmatrix}
T_{g1} \\
T_{g2} \\
T_{f1} \\
T_{ap} \\
T_{f2} \\
T_{bp}
\end{bmatrix}
$$

$$
=
\begin{bmatrix}
(\alpha_{g1}G+h_wT_a+h_{r,g1-s}T_s) \\
(\tau_{g1}\alpha_{g2}GA_h) \\
(\dot{m}c_pT_a) \\
(\tau_{g1}\tau_{g2}\alpha_{ap}GA_h) \\
(\dot{m}c_pT_a) \\
(h_bT_{bp})
\end{bmatrix}
$$

Figure 3.8 : Expressed matrix of the heat balance equations.

3.3.2 Heat Transfer Coefficients

The coefficients of heat transfer by convection, radiation and conduction during heat exchange between the elements of the collector are determined as follows:

The convective heat transfer coefficient of the upper transparent cover due to the wind is suggested by McAdams (1954) [33] as:

$$h_w = 2.8 + 3V_w \qquad\qquad 3.20$$

The radiative heat transfer coefficient from the upper transparent glass layer to sky can be given as:

$$h_{r,g1-s} = \sigma\varepsilon_{g1}(T_{g1} + T_s)(T_{g1}^2 + T_s^2) \qquad\qquad 3.21$$

Where T_s is the sky temperature which can be obtained by Eq. (3.22) [34];

$$T_s = T_a - 6 \qquad\qquad 3.22$$

The radiative and convective heat transfer coefficient between the two transparent glass layers can be expressed as in Eqs. (3.23) and (3.24) respectively [32]:

$$h_{r,g2-g1} = \frac{\sigma(T_{g1}^2 + T_{g2}^2)(T_{g1} + T_{g2})}{1/\varepsilon_{g1} + 1/\varepsilon_{g2} - 1} \qquad\qquad 3.23$$

$$h_{c,g2-g1} = Nu_{g1-g2}\frac{k}{L} \qquad\qquad 3.24$$

It is assumed that $h_{c,g2-g1} = h_{c,g1-g2}$; $h_{r,g2-g1} = h_{r,g1-g2}$ and Nusselt number can be obtained as in Eq. (3.25)[35]:

$$Nu_{g1-g2} = 1 + 1.44\left[1 - \frac{1708}{Ra.\cos\theta}\right]^*\left[1 - \frac{1708(\sin 1.8.\theta)^{1.6}}{Ra.\cos\theta}\right] + \left[(\frac{Ra.\cos\theta}{5830})^{\frac{1}{3}} - 1\right]^* \qquad 3.25$$

Where, θ is the tilt angle of the collector and the superscript ($*$) means that, the values between the brackets are considered to be positive, (should be considered equal zero if the values are negative). It should be noted that Eq. (3.25) can be applied only when $0 \le \theta \le 75$.

On the other hand Eq. (3.26) is valid for $75° < \theta \le 90°$,

$$\text{Nu}_{g1-g2} = \left[1, 0.288(A\sin(\theta)\text{Ra})^{\frac{1}{4}}, 0.039(\sin(\theta)\text{Ra})^{\frac{1}{3}}\right]_{\text{Max}} \qquad 3.26$$

The Rayleigh number (Ra) is calculated as;

$$\text{Ra} = \frac{g\beta\text{Pr}(T_{g2}-T_{g1})H_1^3}{v^2} \qquad 3.27$$

where, Prandtl Number (Pr) and thermal expansion coefficient(β), are given in Eq. (3.28) and Eq.(3.29) respectively;

$$\text{Pr} = \mu.Cp/k \qquad 3.28$$

$$\beta = \frac{1}{T_f} \qquad 3.29$$

where, T_f is the temperature of air located between the glass layers, that can be assumed as the average temperatures of upper and lower glasses, given as in Eq.(3.30);

$$T_f = \frac{T_{g2}+T_{g1}}{2} \qquad 3.30$$

In addition, the specific heat of the air (C_p) can be assumed to be 1000 J/kg.K and other properties of the air (density, thermal conductivity and viscosity of the air) that lies in the temperature range of 280-470 K can be obtained by following Eqs. (3.31), (3.32) and (3.33) [31]:

$$\rho = 3.9147 - 0.016082T_f + 2.9013 \times 10^{-5}T_f^2 - 1.9407 \times 10^{-8} \times T_f^3 \qquad 3.31$$

$$k = (0.0015215 + 0.097459T_f - 3.3322 \times 10^{-5}T_f^2) \times 10^{-3} \qquad 3.32$$

$$\mu = (1.6157 + 0.06523T_f - 3.0297 \times 10^{-5}T_f^2)10^{-6} \qquad 3.33$$

The radiative heat transfer coefficient between the V-corrugated absorber plate and the lower glass layer is calculated as in Eq. (3.34) [36]:

$$h_{r,ap-g2} = \frac{\sigma \varepsilon_{g2} \varepsilon_{ap} (T_{ap}^2 + T_{g2}^2)(T_{ap} + T_{g2})}{\varepsilon_{g2} + \varepsilon_{ap} + \varepsilon_{ap}\varepsilon_{g2}} \qquad 3.34$$

The convective heat transfer coefficient between the V-corrugated absorber plate and the air located in the upper channel is obtained as in Eq. (3.35) [37]:

$$h_{c,ap-f1} = Nu_{ap-f1} \frac{k_1}{D_h} \qquad 3.35$$

Hydraulic diameter of the air channel, the Nusselt number for laminar flow, transitional flow and turbulent flow cases are expressed as in Eqs. (3.36), (3.37), (3.38) and (3.39) respectively:

$$D_h = 2H_2/3 \qquad 3.36$$

$$Nu_{ap-f1} = 2.821 + 0.063 Re_1 \frac{H_2}{L}n \ , \text{for } Re_1 < 2800; \qquad 3.37$$

$$Nu_{ap-f1} = 1.9 \times 10^{-6} Re_1^{1.76} + 112.5 \frac{H_2}{L}n \ , \text{for } 2800 \leq Re_1 \leq 10^4 \qquad 3.38$$

$$Nu_{ap-f1} = 0.0302 Re_1^{0.74} + 0.121 Re_1^{0.74} \frac{H_2}{L}n \ , \text{for } 10^4 \leq Re_1 \leq 10^5 \qquad 3.39$$

The properties of the air located in the upper channel are evaluated by following Eqs. [31]:

$$\rho_1 = 3.9147 - 0.016082 T_{f1} + 2.9013 \times 10^{-5} T_{f1}^2 - 1.9407 \times 10^{-8} \times T_{f1}^3 \qquad 3.40$$

$$k_1 = (0.0015215 + 0.097459 T_{f1} - 3.3322 \times 10^{-5} T_{f1}^2) \times 10^{-3} \qquad 3.41$$

$$\mu_1 = (1.6157 + 0.06523 T_{f1} - 3.0297 \times 10^{-5} T_{f1}^2) \times 10^{-6} \qquad 3.42$$

The Reynolds number for flow in the upper channel is calculated as in Eq. (3.43)[37]:

$$Re_1 = \frac{2\dot{m}}{3\mu_1 W} \qquad 3.43$$

The convective heat transfer coefficient between lower glass layer and the air located in the upper channel is obtained as Eq. (3.44);

$$h_{c,f1-g2} = Nu_{ac,f1-g2} \frac{k_1}{D_h} \qquad \text{3.44}$$

where, it is assumed that $Nu_{ac,f1-g2} = Nu_{ap-f1}$

The convective heat transfer coefficient between V-corrugated absorber plate and the air located in the lower channel is obtained as in Eq. (3.45);

$$h_{c,ap-f2} = Nu_{ap-f2} \frac{k_2}{D_h} \qquad \text{3.45}$$

Where, the properties of the air located in the lower channel are evaluated by the following Eqs. (3.46), (3.47) and (3.48) [31]:

$$\rho_2 = 3.9147 - 0.016082 T_{f2} + 2.9013 \times 10^{-5} T_{f2}^2 - 1.9407 \times 10^{-8} \times T_{f2}^3 \qquad \text{3.46}$$

$$k_2 = (0.0015215 + 0.097459 T_{f2} - 3.3322 \times 10^{-5} T_{f2}^2) \times 10^{-3} \qquad \text{3.47}$$

$$\mu_2 = (1.6157 + 0.06523 T_{f2} - 3.0297 \times 10^{-5} T_{f2}^2) \times 10^{-6} \qquad \text{3.48}$$

In addition, the Nusselt number for laminar flow, transitional flow and turbulent flow in the lower air channel are given in Eqs. (3.49), (3.50) and (3.51) respectively:

$$Nu_{ap-f2} = 2.821 + 0.063 Re_2 \frac{H_2}{L} n \text{ , for } Re_2 < 2800; \qquad \text{3.49}$$

$$Nu_{ap-f2} = 1.9 \times 10^{-6} Re_2^{1.76} + 112.5 \frac{H_2}{L} n \text{ , for } 2800 \leq Re_2 \leq 10^4 \qquad \text{3.50}$$

$$Nu_{ap-f2} = 0.0302 Re_2^{0.74} + 0.121 Re_2^{0.74} \frac{H_2}{L} n \text{ , for } 10^4 \leq Re_2 \leq 10^5 \qquad \text{3.51}$$

The Reynolds number for air flow in the lower channel is calculated as [37]:

$$Re_2 = \frac{2\dot{m}}{3\mu_2 W} \qquad \text{3.52}$$

The radiative heat transfer coefficient between the V-corrugated and flat absorber plate is obtained by Eq. (3.53) [31]:

$$h_{r,ap-bp} = \frac{\sigma \varepsilon_{bp} \varepsilon_{ap} (T_{ap}^2 + T_{bp}^2)(T_{ap} + T_{bp})}{\varepsilon_{bp} + \varepsilon_{ap} + \varepsilon_{bp} \varepsilon_{ap}} \qquad \text{3.53}$$

Total thermal resistance for back of the collector is given in Eq. (3.54):

$$R = \sum \frac{t_i}{k_i} \quad \& \quad R = \frac{t_{bp}}{K_{bp}} + \frac{t_{ins}}{k_{ins}} + \frac{t_{wood}}{k_{wood}} + \frac{t_{Ex,c}}{k_{Ex,c}} + \frac{1}{h_w} \tag{3.54}$$

Overall thermal transmittance of back elements h_b of the collector is obtained as the following equation:

$$h_b = \frac{1}{R} \tag{3.55}$$

3.3.3 Matlab Code

To evaluate the total useful heat and the area required to meet a specific heating load, it is necessary to determine the temperature values for each element of the solar air collector. Matlab code is constructed to solve the linear heat balance equations by using matrix inversion method that are expressed in the form of $[A] * [T] = [B]$ which is shown in Figure 3.8.

Thermophysical properties and measured parameters with assumed initial temperatures of each element ($T_{g1}, T_{g2}, T_{f1}, T_{f2}, T_{ap}, T_{bp}$) are introduced into the Matlab code to determine all initial values of heat transfer coefficents. Accordingly, the code obtains new temperature values for the new iteration and this continues until the preset condition is satisfied. The flowchart for the Matlab code is shown in Figure 3.9.

```
                              ┌─────────────────┐
                              │      Start      │
                              └────────┬────────┘
                                       │
                                       ▼
                    ┌──────────────────────────────────────┐
                    │  Setting thermophysical properties    │
                    │     and operating parameters of       │
                    │           a D-P/GVCPSAC               │
                    └──────────────────┬───────────────────┘
                                       │
                                       ▼
                    ┌──────────────────────────────────────┐
                    │       Assume initial temperatures      │
                    │ ( Tg1 , Tg2 , Tf1 , Tf2 , Tap , Tbp ) │
                    └──────────────────┬───────────────────┘
                                       │
                   ┌───────────────────▼──────────────────┐
                   │     Compute heat transfer coefficients │
                   │      by utilizing Eqs.(3.20) to (3.55) │
                   │                respectively            │
                   └───────────────────┬──────────────────┘
                                       │
                                       ▼
            ┌──────────────────────────────────────────────────────┐
            │  Compute new temperatures ( Tg1 , Tg2 , Tf1 , Tf2 ,   │
            │                             Tap , Tbp )               │
            │ by using energy balance equations,that are expressed  │
            │                   as matrix (6 X 6)                   │
            └──────────────────────────────┬───────────────────────┘
                                           │
                                           ▼
      No        ◇──────────────────────────────────────◇
      ◄─────────        If
                (New temperature- Old temperature)
                           < 0.001
                ◇──────────────────────────────────────◇
                                           │ Yes
                                           ▼
            ┌──────────────────────────────────────────────────────┐
            │  Compute Tf1out ,Tf2out , qu1 ,qu2 ,Qu total          │
            │   Number of solar collectors and Area required        │
            └──────────────────────────────┬───────────────────────┘
                                           │
                                           ▼
                              ┌─────────────────┐
                              │      Stop       │
                              └─────────────────┘
```

Figure 3.9 : Flowchart of Matlab code.

Chapter 4

EXPERIMENTAL PROCEDURE

4.1 Introduction

In the preceding chapter, the mathematical model for the considered solar collector is developed and proposed to be solved by Matlab software. The useful heat output is used together with the outputs from the Energy Plus simulations of the target office space (maximum value of heating load) in order to evaluate the required number of solar collectors for meeting the heating demand of the office space.

Comparing the outputs of the Matlab code for the various parameters ($T_{g1}, T_{g2}, T_{f1}, T_{f2}, T_{ap}, T_{bp}, T_{f1o}, T_{f2o}$) and the monitored values of the same parameters is one of the aims and objectives of this study. In this chapter experimental procedure is explained for monitoring the parameters that is used for comparison.

National Bureau of Standards (NBS) [38] and ASHRAE Standard (93-77) [39] are International standards of the thermal performance testing methods for solar air collectors, which are providing the essential conditions and required procedures of this test. Some of this essential conditions and procedures are [40]:

- The collector fan should be operated and controlled prior to the testing and monitoring.
- The pyranometer should be placed on the collector.

- All the necessary measurement devices for monitoring the ambient conditions (air temperature, wind speed etc.), mass flow rate, pressure and pressure drop through the collector, should be available.

- Temperature measurement tools should be available and connected to the target elements of the collector.

4.2 Preparation of Solar Air Collector for Experiments

Experimental work is started by maintenance of the D-F/GVCPSAC that is produced and tested previously in the Mechanical Engineering Department. Figure 4.1 illustrates the preparation stages of the collector, which is retrofitted for experimental test of this study[8].

Figure 4.1: (A, B, C) the preparation stages of a D-F/GVCPSAC[8].

The elements of the collector are wore and damaged by being exposed to open air without any maintenance for a long time. The collector is transferred from top of the building to the workshop for maintenance which included the change of the transparent covers that are broken. In addition, insulation material (2 cm polystyrene layer) at the back of the collector is renewed.

The main components of D-F/GVCPSAC are: 2 mm-thick sheet metal back absorber plate, two 3 mm-thick transparent glass covers and a V-corrugated sheet metal absorber plate that is formed with groove angles of 60° and located between the lower glass and back absorber plate. The collector has an external protective cover that is manufactured from galvanized steel with dimensions: length 200 cm, width 100 cm and thickness 20 cm. The model of the collector with its outer dimensions is shown in Figure 4.2.
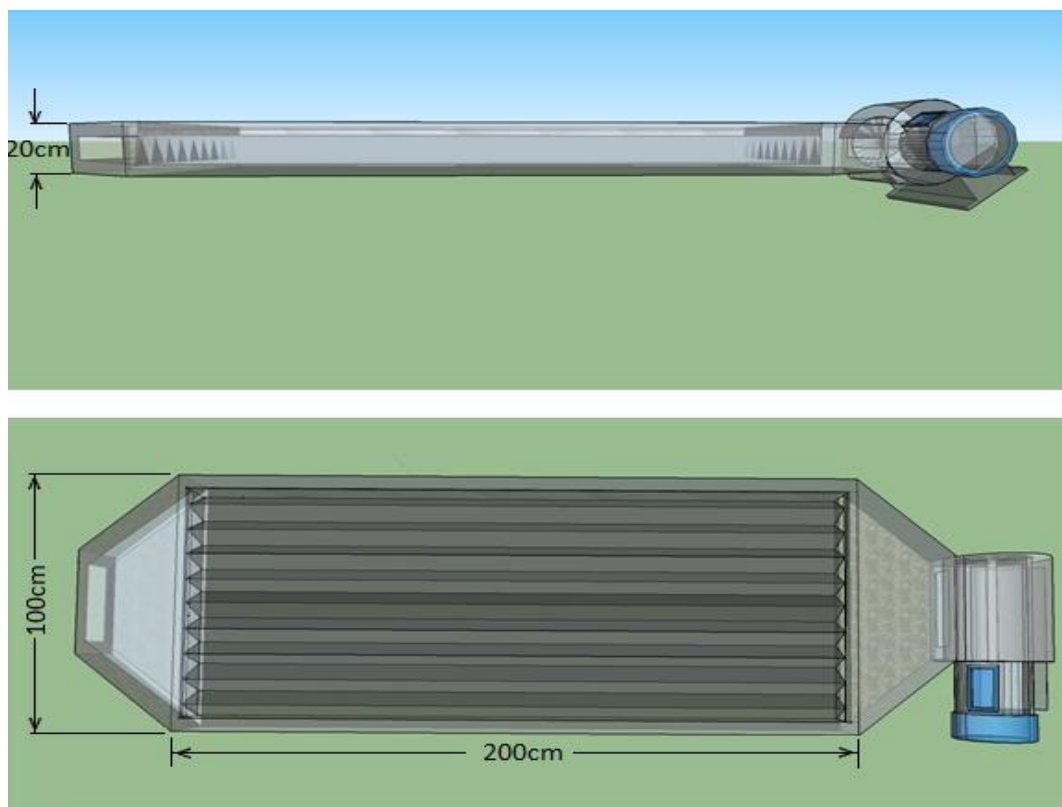
Figure 4.2 : Model of the D-F/GVCPSAC.

Table 3.3 in the preceding chapter includes detailed description of the components of D-F/GVCPSAC.

The air through the channels of the collector will be supplied by electric fan with motor type (OBR 200 M-2K) as illustrated in Figure 4.3. The mass flow rate of the air is controlled by an electric resistor tool, which controls the input voltage (60 - 220V).

Figure 4.3: Photograph of collector Fan.

4.3 Measurement Equipment

4.2.1 Hand Held Data Logger

For recording the temperature of each element of the collector, ambient temperature, the wind speed and outlet air velocity from the collector channels, the hand held data logger; Pasco GLX is used. This data logger can be used with various sensors e.g. anemometer, temperature sensor etc. In the testing, anemometer sensor is employed for wind speed and outlet air velocity measurements, whereas temperature sensors are used to measure ambient air temperature and temperatures of the collector elements.

4.2.2 Temperature Sensors

To measure the temperature of each element of the collector, nine temperature sensors (Fast Response Temperature Probe, PS-2135) are used with five data loggers (Xplorer GLX type). Each data logger has two temperature ports at the left of the screen to connect the sensors. The temperature sensors are able to measure temperatures in the range of -30°C to approximately 105 °C with accuracy of ±0.5°C [41]. Figure 4.4 shows the hand held data logger, Xplorer Pasco GLX and temperature sensor.

Figure 4.4: Hand held data logger Xplorer Pasco GLX.

4.2.3 Anemometer

Anemometer sensor is employed to measure the local wind speed and the exit air speed from the channels of the solar air collector which are required parameters for running the Matlab code in order to solve the mathematical model for useful heat. Figure 4.5 illustrates the anemometer sensor which is coupled with hand held data logger.

Figure 4.5: Photograph of Anemometer sensor.

4.2.4 Data Acquisition System

In this study, the data acquisition system OMB-DAQ-3000 is utilized with pyranometer to measure the global solar irradiation, which is shown in figure 4.6.

The data acquisition system is connected to a desktop computer by a USB wire. The software package of the Data Acquisition system is installed on this computer.
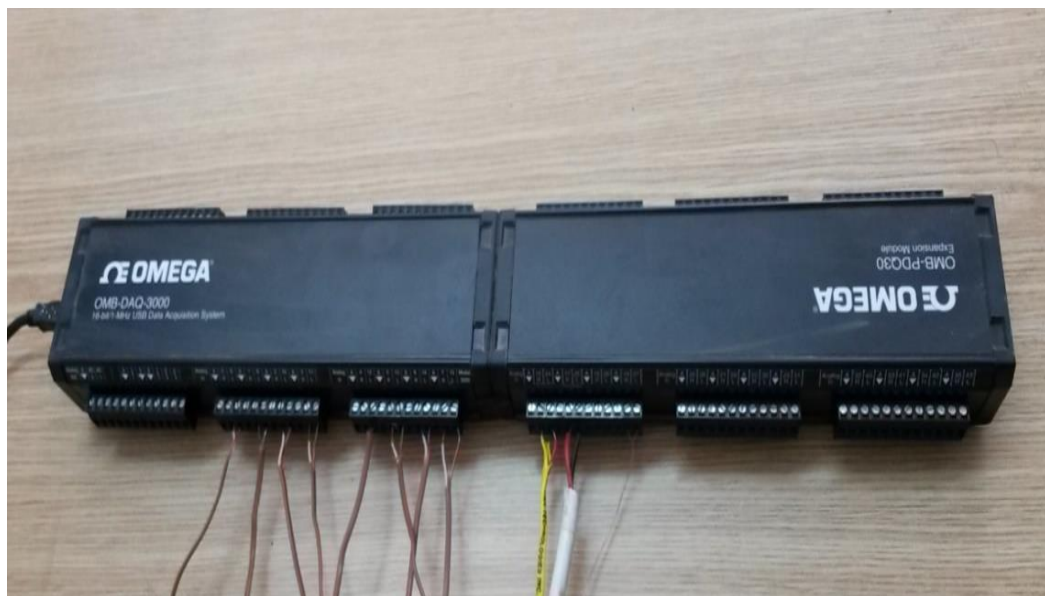
Figure 4.6: Data Acquisition system OMB-DAQ-3000.

4.2.5 Pyranometer

A pyranometer is utilized to measure the global solar irradiation. The pyranometer is shown in Figure 4.7. The solar radiation is absorbed in the thermopile sensor of the pyranometer and activates the sensor to generate a voltage signal proportional with amount of the incident solar irradiance. This device is able to work with 180 degrees of view [42]. The pyranometer is placed on the collector with the same slope as the collector as shown in Figure 4.10 and connected to Data Acquisition system.

Figure 4.7: Photograph of pyranometer device.

4.4 Experimental Setup

The collector is tested at Famagusta, N. Cyprus (35.125°N and 33.95°E). The surface azimuth of the collector is set as 0° thus; the collector is directed to the south. The tilt angle of the collector is 45°. The sensors are positioned at different parts in the collector as illustrated in Figure 4.8, Figure 4.9 and Figure 4.10 for measuring the following:

- The ambient temperature (T_a), (inlet air temperature $T_a = T_{f1i} = T_{f2i}$),

- The upper glass cover temperature (T_{g1}),

45

- The lower glass cover temperature (T_{g2}),

- The V-corrugated absorber plate temperature (T_{ap}),

- The back absorber plate temperature (T_{bp}),

- The air temperature located in the middle of upper channel (T_{f1}),

- The air temperature located in the middle of lower channel (T_{f2}),

- Exit air temperature from the upper channel (T_{f1o}),

- Exit air temperature from the lower channel (T_{f2o}),

- Wind speed (V_w), the air mass flow rate (ṁ) and global solar irradiation (G).
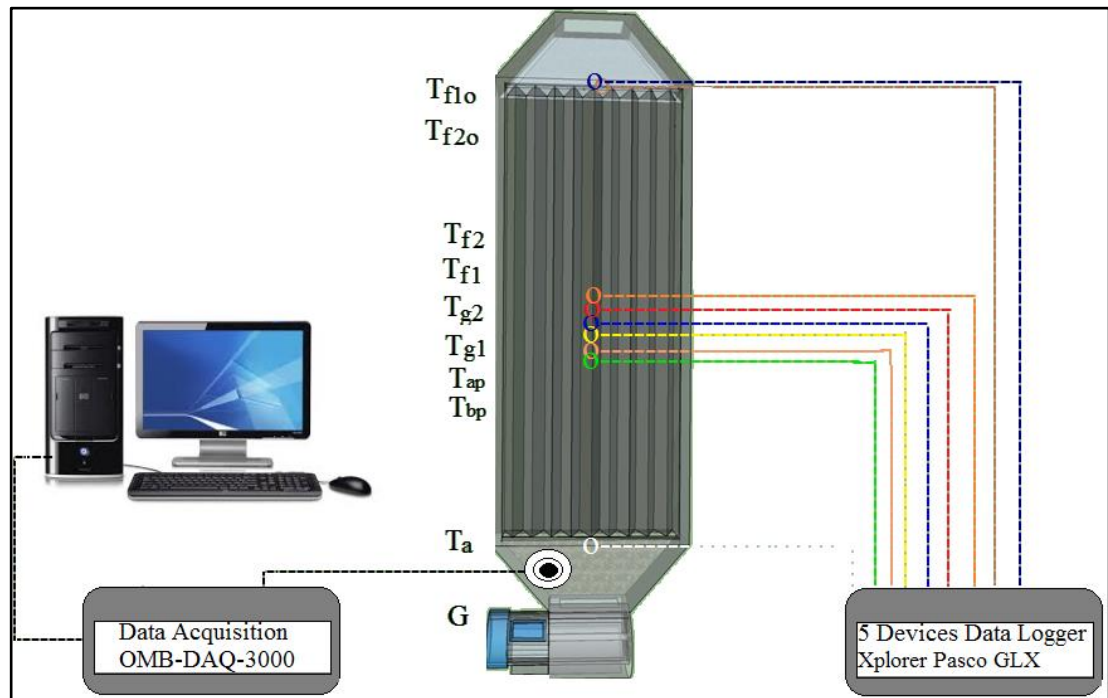
Figure 4.8: Schematic of the experimental setup.
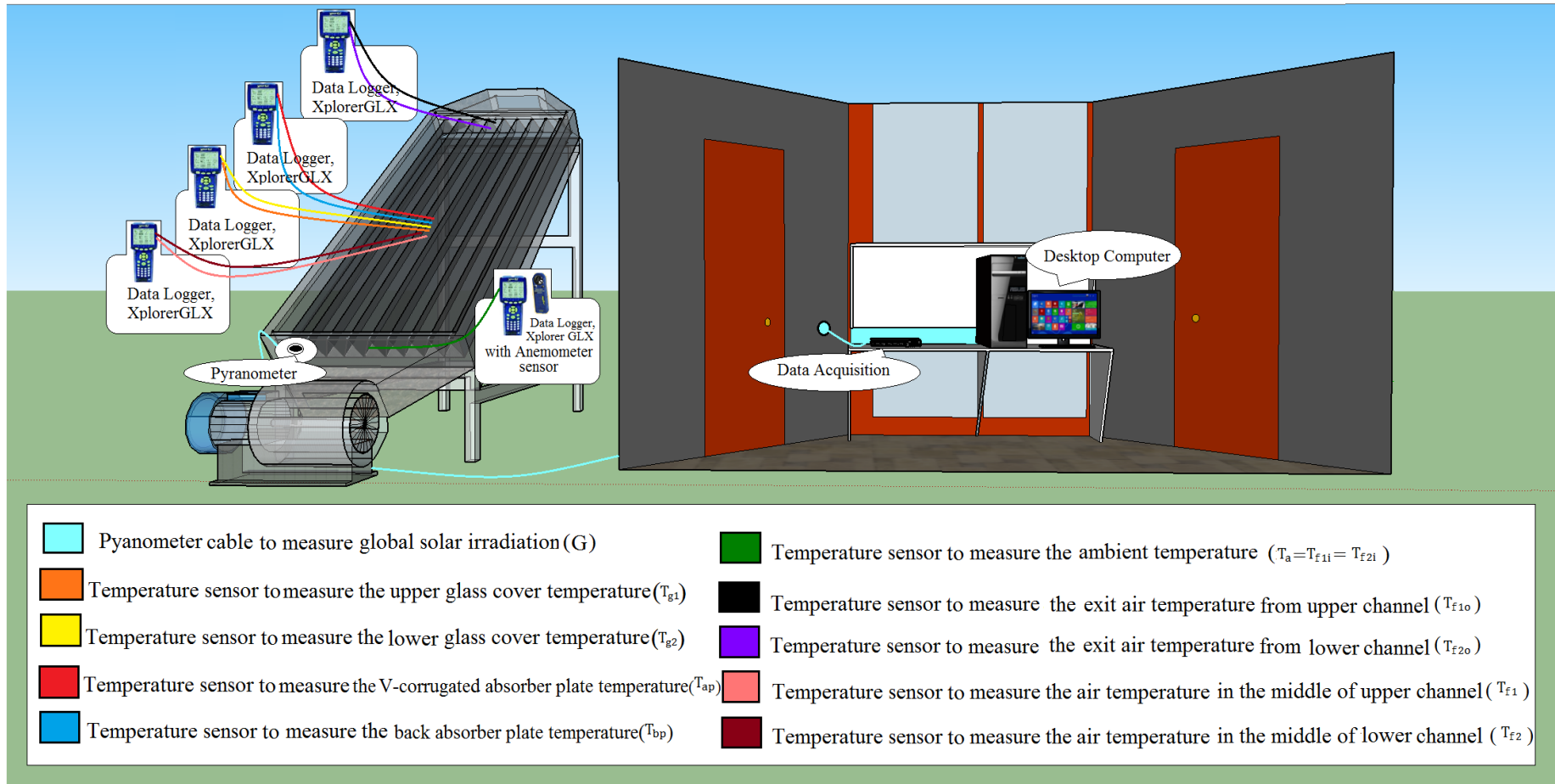
Figure 4.9: 3D visualization of the experimental setup.

Figure 4.10: Photograph of D-F/GVCPSAC.

The measured wind speed is a required parameter in the Matlab code for evaluating the convection heat transfer coefficient ($h_w = 2.8 + 3V_w$, see Chapter 3) from the top and back of the collector. Also, global solar radiation and air mass flow rate measurements are required parameters in the Matlab code for evaluating the useful heat output.

The equations (3.8a), (3.8b), (3.9a) and (3.9b) that are given in the preceding chapter is used to determine the useful thermal energy output from upper air channel ($\dot{q}_{u1,Ex}$), the useful thermal energy output from lower air channel ($\dot{q}_{u2,Ex}$), the total useful thermal energy output ($\dot{Q}_{tu,Ex}$) and the thermal efficiency of the collector ($\eta_{TH,Ex}$), from the experimental measurements.

These equations are reproduced as follows:

$$\dot{q}_{u1,Ex} = \dot{m}_1 c_p (T_{f1o} - T_{f1i}), \hspace{4cm} 4.1$$

$$\dot{q}_{u2,Ex} = \dot{m}_2 c_p (T_{f2o} - T_{f2i}), \hspace{4cm} 4.2$$

$$\dot{Q}_{tu,Ex} = \dot{q}_{u1,Ex} + \dot{q}_{u2,Ex}, \hspace{4cm} 4.3$$

$$\eta_{TH,Ex} = \frac{\dot{Q}_{tu,Ex}}{GA_h} \times 100, \hspace{4cm} 4.4$$

Where, c_p, G, A_h and $\dot{m}$ are the specific heat of the air, global solar irradiation, absorber surface area of the collector and the air mass flow rate ($\dot{m}$) respectively.

Air mass flow rate can be obtained by the following equation:

$$\dot{m}_1 = \rho_{1o}. V. A_c / 2, \hspace{4cm} 4.5$$

$$\rho_{1o} = 3.9147 - 0.016082 T_{f1o} + 2.9013 \times 10^{-5} T_{f1o}^2 - 1.9407 \times 10^{-8} \times T_{f1o}^3 \quad 4.6$$

$$\dot{m}_2 = \rho_{2o}. V. A_c / 2 \hspace{4cm} 4.7$$

$$\rho_{2o} = 3.9147 - 0.016082 T_{f2o} + 2.9013 \times 10^{-5} T_{f2o}^2 - 1.9407 \times 10^{-8} \times T_{f2o}^3 \quad 4.8$$

Where ρ, V and A_c are the density of air, the air velocity in the collector channel and the cross sectional area of the collector channels respectively.

The thermal efficiency of the collector can be written as:

$$\eta_{TH,Ex} = \frac{c_p(\dot{m}_1(T_{f1o} - T_{f1i}) + \dot{m}_2(T_{f2o} - T_{f2i}))}{G.A_h} * 100, \hspace{2cm} 4.9$$

Where; $T_{f1i} = T_{f2i} = T_a$.

Chapter 5

RESULTS & DISCUSSION

5.1 Energy plus Simulation Results

The office building that is intended to be served by the solar collector has been modeled and simulated by Energy Plus software in order to calculate the heating load. The weather data for Larnaca is chosen to be used in Energy Plus as it is the nearest location to Famagusta. The simulated period is for three months, from the first of November until the end of January. The simulation results revealed the fluctuations in the daily average values of the building heating load during the period which is illustrated in figures 5.1. The maximum value of the evaluated load is recorded in sixteen of January which is approximately 4564 W.

The maximum load that is evaluated by the program is accepted as the design heating load of the office space. This load is used together with the evaluated total useful heat output from the collector (from Matlab code) to find the number of solar collectors that are required to cover the heating demand of the space during a typical winter day.
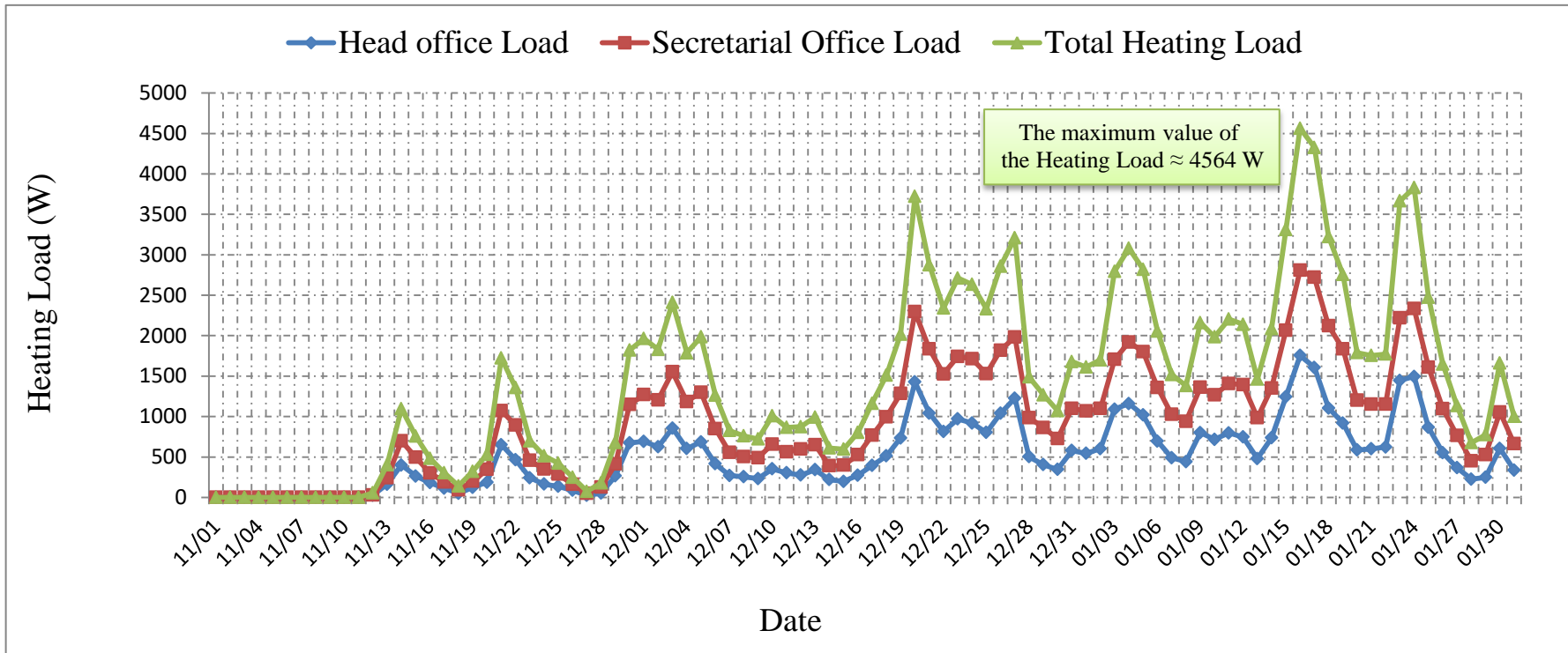
Figure 5.1: The daily heating loads of the MEDC Office during the simulation period.

5.2 Results and Data Analysis

In order to run the Matlab code for evaluating the useful heat, thermal efficiency, etc. various environmental parameters such as wind speed (V_w), ambient temperature (T_a) and global solar radiation (G) are required to be inputted. These parameters have been recorded during 15**th** December 2016 from 09:20 until 16:00 for every 5minutes (i.e. time step=5minutes). The mean of six values are evaluated for representing every half hour. Figure 5.2 and Figure 5.3 show the data for every half hour for those parameters for 15th December 2016 that are used in the Matlab code. Notice that the values before 11:00 and subsequent to 14:30 are not given in the figures below since, the monitored results revealed that the thermal inertia has a significant effect on the thermal performance of the collector during that period causing substantial mismatch between the measured and simulated values. This is expected as the mathematical model of D-F/GVCPSAC is constructed based on the negligible thermal inertia of each component of the collector.

	11:00	11:30	12:00	12:30	13:00	13:30	14:00	14:30
Ta	290.08	290.37	291.15	291.97	292.12	292.30	291.58	291.07
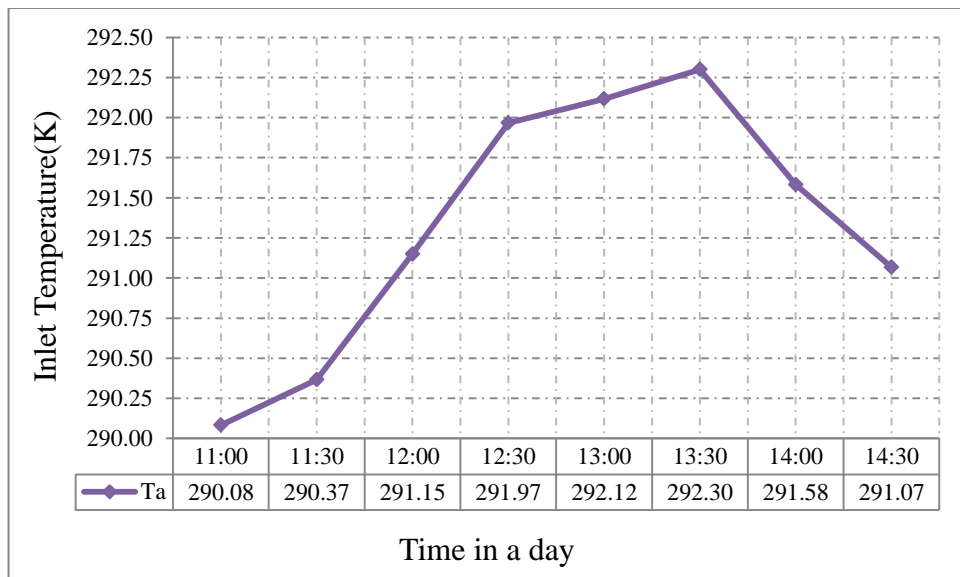
Figure 5.2: Measured inlet temperature.
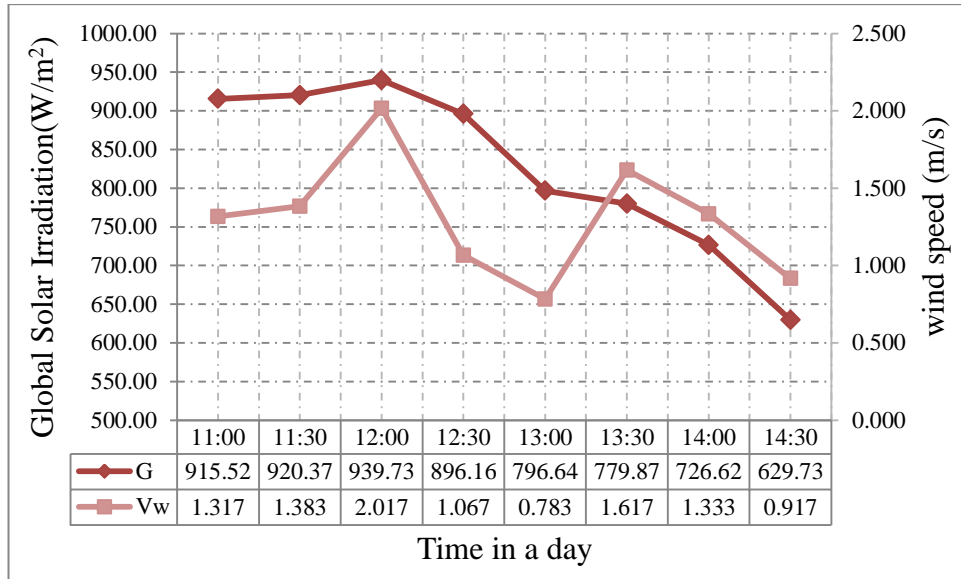
Figure 5.3: Measured values of the wind speed and global solar radiation.

The other parameters that are necessary for the Matlab code are given in table 5.1.

Table 5.1: Inputted parameters in Matlab code.

P	Value	P	Value	P	Value
W	0.9m	L	1.94m	H_1	0.01m
H_2	0.1m	t_{bp}	0.002m	t_{ins}	0.02m
t_{wood}	0.04m	$t_{Ex,c}$	0.002m	k_{bp}	79.5W/m.K
k_{wood}	0.1W/m.K	k_{ins}	0.045W/m.K	$k_{Ex,c}$	79.5W/m.K
α_{ap}	0.9	α_{g1}	0.06	α_{g2}	0.06
τ_{g1}	0.9	τ_{g2}	0.9	c_p	1000 J/Kg.K
ε_{g1}	0.88	ε_{g2}	0.88	ε_{ap}	0.9
ε_{bp}	0.9	Q_{office}	4564W	g	$9.8m/s^2$
σ	$5.668*10\text{-}8 \ W/m^2.K^4$	$\dot{m}$	0.2 kg/s	π	3.14159265

The flow rate of the air is set according to the motor rpm. The minimum motor rpm is resulting flow speed of 1.2 m/s, leading to a mass flow rate of 0.13 kg/s. The Reynolds number in the channel with this air speed is 4.9265e+03, corresponding to transitional flow. The motor rpm set to result in air velocity of 1.8 m/s which gives flow rate of 0.2 kg/s. This is done in order to avoid running the motor speed at its minimum rpm. With this flow rate Reynolds number in the upper and lower channels are 8.2067e+03 and 7.5792e+03 respectively corresponding to transitional flow regime. This leads the use of equations 3.38 and 3.50 for calculating Nu number.

The temperature of each element of the collector, the useful heat output from upper and lower channel and the thermal efficiency are shown in Figure 5.4 until Figure 5.14. The required number of collectors and the area to meet the target heating load that is obtained by the code and the experimental analysis are shown in Table 5.2. Note that the values are given for every half hour.

The temperature of the collector elements; upper glass, lower glass, v-corrugated plate and back plate are shown in Figure 5.4, Figure 5.5, Figure 5.6 and Figure 5.7 respectively. Once those figures are investigated, it is seen that the simulation results are having similar trend as the experimental ones. It is clear that there is some discrepancy between the measured and simulated values. In some hours these discrepancies are very low whereas in some they are at significant order. The average of the differences of the simulated and monitored temperatures for upper glass cover, lower glass cover, v-corrugated plate and back plate are 1.4, 1.6, 2.8 and 2.0 K respectively.
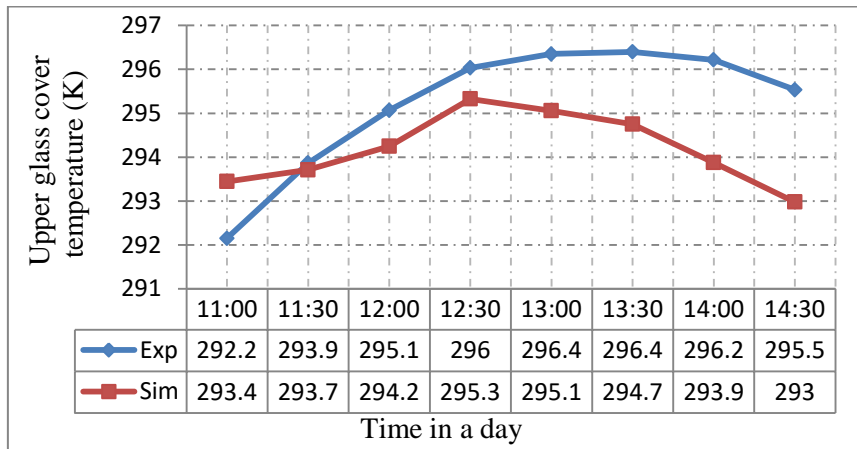
Figure 5.4 : Upper glass cover temperatures obtained from simulations and measurements.

	11:00	11:30	12:00	12:30	13:00	13:30	14:00	14:30
Exp	292.2	293.9	295.1	296	296.4	296.4	296.2	295.5
Sim	293.4	293.7	294.2	295.3	295.1	294.7	293.9	293
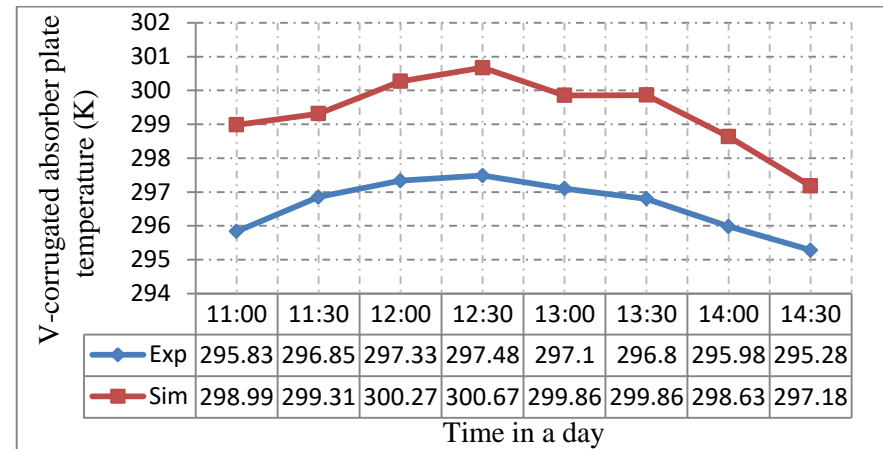
Figure 5.6 : V- corrugated absorber plate temperatures obtained from simulations and measurements.

	11:00	11:30	12:00	12:30	13:00	13:30	14:00	14:30
Exp	295.83	296.85	297.33	297.48	297.1	296.8	295.98	295.28
Sim	298.99	299.31	300.27	300.67	299.86	299.86	298.63	297.18
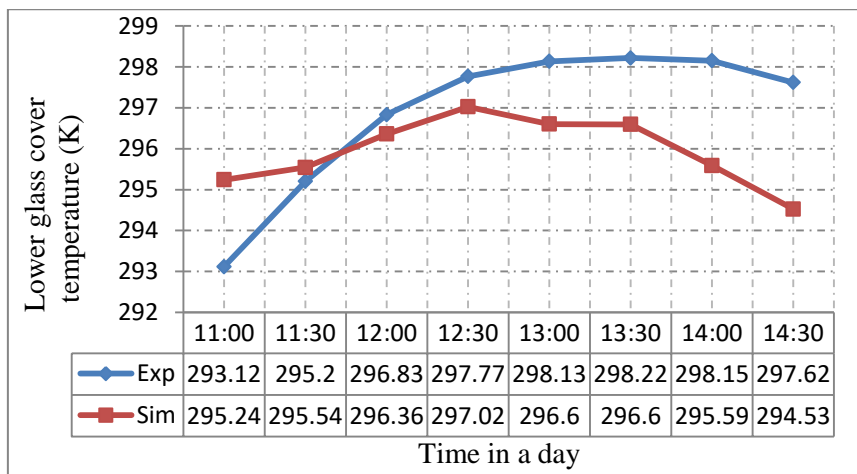
Figure 5.5: Lower glass cover temperatures obtained from simulations and measurements.

	11:00	11:30	12:00	12:30	13:00	13:30	14:00	14:30
Exp	293.12	295.2	296.83	297.77	298.13	298.22	298.15	297.62
Sim	295.24	295.54	296.36	297.02	296.6	296.6	295.59	294.53
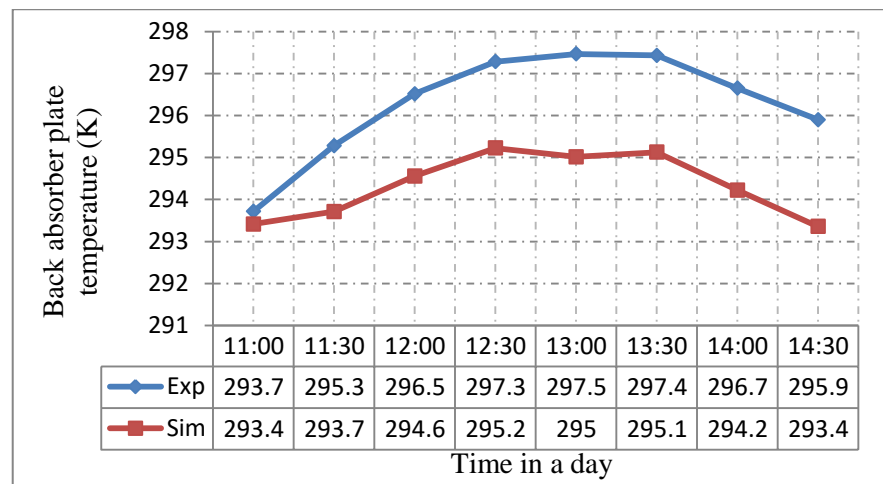
Figure 5.7 : Back absorber plate temperatures obtained from simulations and measurements.

	11:00	11:30	12:00	12:30	13:00	13:30	14:00	14:30
Exp	293.7	295.3	296.5	297.3	297.5	297.4	296.7	295.9
Sim	293.4	293.7	294.6	295.2	295	295.1	294.2	293.4

Once the air temperatures at the middle and at the exit of the upper and lower channel obtained from simulations and measurements shown in Figure 5.8, Figure 5.9, Figure 5.10 and Figure 5.11 are investigated, it is seen that the simulations and the measurements agreeing with some discrepancy, however the agreement is better than those for the collector elements. The average of the differences between the measured and simulated values are 0.6, 2.5, 1.3, and 1.7 K for the air temperatures at the middle and the exit of upper channel then for the air temperatures at the middle and exit of the lower channel respectively. The better agreement between the simulation results and the experiments for the air temperatures than the collector elements is due to the quick response of the air to the changes resulting in less effective dynamic behavior.

It is expected to have some disagreement between the simulations and the measured values. First of all the Matlab code is not taking the thermal inertia and the dynamic behavior of the collector into consideration. The response of the collector elements should be accounted in order to obtain more realistic results. In addition, the actual properties of the collector elements such as glass emissivity and transmittivity, absorber plate absorptivity, thermal conductivity etc. are likely to have values that are different those employed for Matlab simulation. Although the values for these properties are found from reliable sources and catalogs they are hardly matching with the actual case. Furthermore the accuracies of the monitoring equipment are thought to have substantial effect on these discrepancies. An uncertainty analysis is presented in the next section in order to measure the effect of the equipment accuracies in the experimental results.
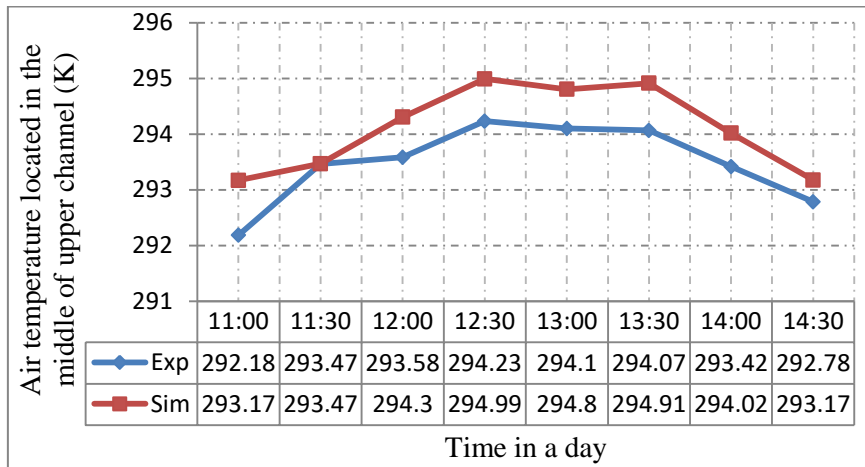
Figure 5.8 : Air temperatures located in the middle of upper channel obtained from simulations and measurements.

	11:00	11:30	12:00	12:30	13:00	13:30	14:00	14:30
Exp	292.18	293.47	293.58	294.23	294.1	294.07	293.42	292.78
Sim	293.17	293.47	294.3	294.99	294.8	294.91	294.02	293.17

Figure 5.10 : Exit air temperatures from the upper channel obtained from simulations and measurements.

	11:00	11:30	12:00	12:30	13:00	13:30	14:00	14:30
Exp	292.6	293.9	294.9	295.5	295.3	295.2	294.2	293.7
Sim	296.3	296.6	297.5	298	297.5	297.5	296.5	295.3

Figure 5.9 : Air temperatures located in the middle of lower channel obtained from simulations and measurements.

	11:00	11:30	12:00	12:30	13:00	13:30	14:00	14:30
Exp	291.2	292.2	292.3	293.2	293.3	293.5	293	292.5
Sim	293	293.3	294.2	294.8	294.7	294.8	293.9	293.1
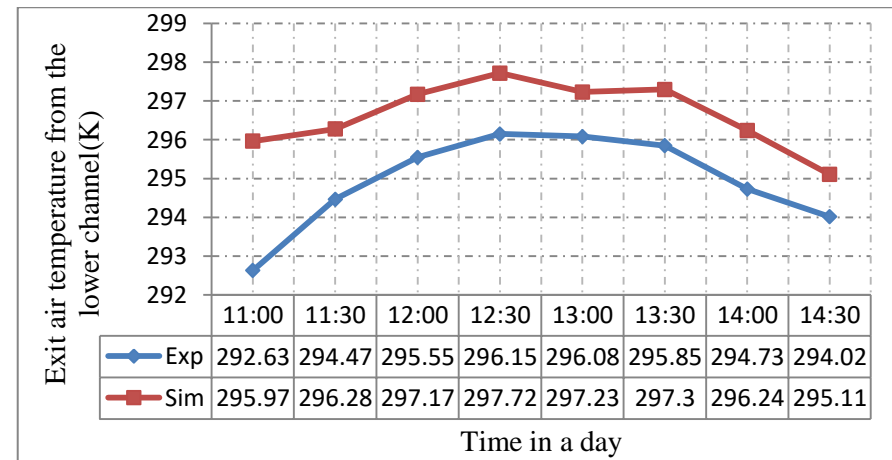
Figure 5.11 : Exit air temperatures from the lower channel obtained from simulations and measurements.

	11:00	11:30	12:00	12:30	13:00	13:30	14:00	14:30
Exp	292.63	294.47	295.55	296.15	296.08	295.85	294.73	294.02
Sim	295.97	296.28	297.17	297.72	297.23	297.3	296.24	295.11

Figure 5.12 and Figure 5.13 shows the useful heat output from upper and lower channel, and the thermal efficiency of the collector obtained from simulations and measurements. It is seen that, significant discrepancies are observed in conjunction with the disagreements in the exit air temperatures, since the useful heat output from both of collector channels and the thermal efficiency are obtained from below equations;

$$\dot{q}_{u1,Ex} = \dot{m}_1 c_p (T_{f1o} - T_{f1i}),$$

$$\dot{q}_{u2,Ex} = \dot{m}_2 c_p (T_{f2o} - T_{f2i}),$$

$$\dot{Q}_{tu,Ex} = \dot{q}_{u1,Ex} + \dot{q}_{u2,Ex},$$

$$\eta_{TH,Ex} = \frac{\dot{Q}_{tu,Ex}}{GA_h} \times 100$$

It's clear, one degree disagreement multiple in the specific heat of the air which equal 1000 J/kg.K will generate a significant discrepancies in both of the useful heat and the thermal efficiency results.
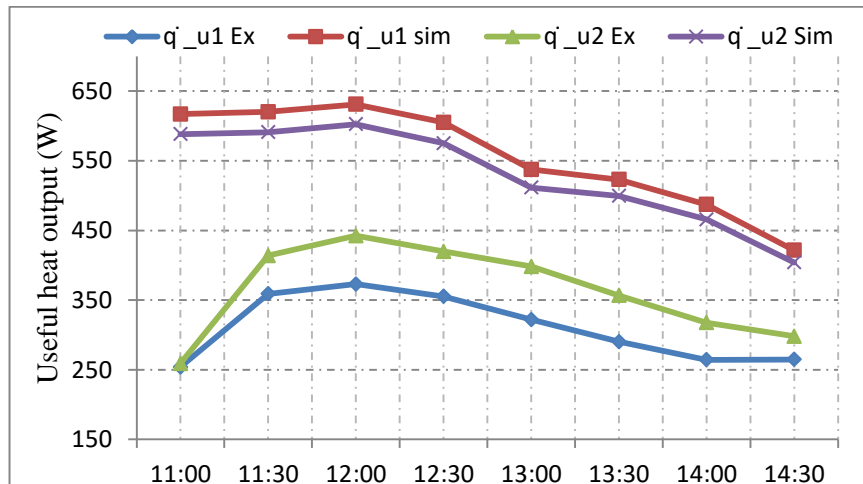
Figure 5.12 : Useful heat output from upper and lower channel obtained from simulations and measurements.
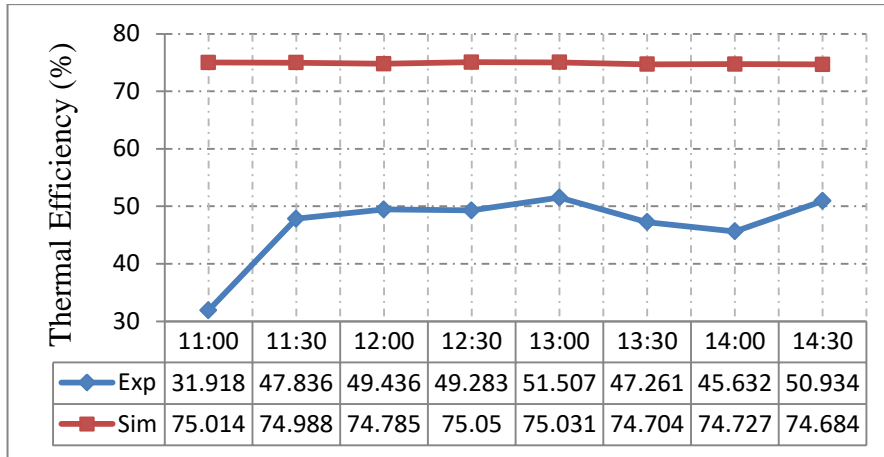
Figure 5.13 : The thermal efficiency of the collector obtained from simulations and

measurements.

Table 5.2 shows the number of collectors and the required area to cover heating load of the MEDC Office for every half hour that is obtained by monitoring and simulation. The number of collector and the corresponding area that is necessary to supply the load is taken as the maximum number which resulted in as 9 collectors with 16 m^2 for the real case (monitoring) and 6 collectors with 10 m^2 for simulations.

Table 5.2: Number of collectors and the required area to meet target load.

Time	$Nu'_C Ex$	$Nu'_C Sim$	$A_{total} Ex$	$A_{total} Sim$
11:00	8.899588	3.7867	15.61878	6.6456
11:30	5.906808	3.7680	10.36645	6.6129
12:00	5.597833	3.7004	9.824197	6.4943
12:30	5.888268	3.8666	10.33391	6.7860
13:00	6.337788	4.3508	11.12282	7.6356
13:30	7.0557	4.4638	12.38275	7.8340
14:00	7.843264	4.7894	13.76493	8.4055
14:30	8.107916	5.5295	14.22939	9.7043
Max	$\approx$ 9 collectors	$\approx$ 6 collectors	$\approx$ 16 m^2	$\approx$ 10 m^2

5.3 Uncertainty Analysis

Comparison of the obtained results by simulations and measurements revealed that, there are significant discrepancies between them. As stated in the preceding section one of the reason for this difference is due to the effect of the accuracies of the employed equipment in the experimental results. In this section an uncertainty analysis of the experimental results (for useful heat) are carried out. Kline and McClintock presented method to evaluate the uncertainty of experimental results [43].

Suppose that the result R is function of several variables; $R = R(x_1, x_2, x_3, \ldots \ldots x_n)$ and $W_{x_1}, W_{x_2}, W_{x_3}, \ldots \ldots, W_{x_n}$ are the uncertainties in the independent variables. Then the uncertainty in the result R can be obtained as [44];

$$W_R = \left[\left\{ \left(\frac{\partial R}{\partial x_1} \right)^2 \times \left(W_{x_1} \right)^2 \right\} + \left\{ \left(\frac{\partial R}{\partial x_2} \right)^2 \times \left(W_{x_2} \right)^2 \right\} + \cdots + \left\{ \left(\frac{\partial R}{\partial x_n} \right)^2 \times \left(W_{x_n} \right)^2 \right\} \right]^{0.5} \quad 5.1$$

This method is applied on the equations (4.1) to (4.9) to find the uncertainty of the useful heat output of the collector.

- The uncertainty in the air density $W_{\rho_{1o}}$ and $W_{\rho_{1o}}$ (For the air located at the exit of the upper and lower channel) is evaluated as follows:

  Air density is a function of temperature ($\rho_{1o} = f(T_{f1o})$ and $\rho_{2o} = f(T_{f2o})$) and the accuracy of the utilized temperature sensors are ±0.5°C, so $W_{T_f} = \pm\, 0.5\ °C$ [41].

- The air density at exit of the upper channel is evaluated by;

  $\rho_{1o} = 3.9147 - 0.016082 T_{f1o} + 2.9013 \times 10^{-5} T_{f1o}^2 - 1.9407 \times 10^{-8}\ T_{f1o}^3$

  So,

60

$$\frac{\partial \rho_{1o}}{\partial T_{f1o}} = (-0.016082) + 5.8026 \times 10^{-5} T_{f1o} - 5.8221 \times 10^{-8} T_{f1o}^2$$

$$W_{\rho_{1o}} = \left[\left(\frac{\partial \rho_{1o}}{\partial T_{f1o}} \right)^2 * \left(W_{T_{f1o}} \right)^2 \right]^{0.5} \qquad\qquad 5.2$$

- The air density at the exit of the lower channel is found by;

$$\rho_{2o} = 3.9147 - 0.016082 T_{f2o} + 2.9013 \times 10^{-5} T_{f2o}^2 - 1.9407 \times 10^{-8} \, T_{f2o}^3$$

So,

$$\frac{\partial \rho_{2o}}{\partial T_{f2o}} = (-0.016082) + 5.8026 \times 10^{-5} T_{f2o} - 5.8221 \times 10^{-8} T_{f2o}^2, \text{ then}$$

$$W_{\rho_{2o}} = \left[\left(\frac{\partial \rho_{2o}}{\partial T_{f2o}} \right)^2 * \left(W_{T_{f2o}} \right)^2 \right]^{0.5} \qquad\qquad 5.3$$

- The uncertainty in the air mass flow rate $W_{\dot{m}_1}$ and $W_{\dot{m}_2}$ is evaluated as follows:

  Mass flow rate is a function of density and air velocity ($\dot{m}_1 = f(\rho_{1o}, V)$ and $\dot{m}_2 = f(\rho_{2o}, V)$). The uncertainty in air velocity is $W_V = \pm(3 \%$ of reading $+0.2$ m/s) [45].

- The air mass flow rate in the upper channel is obtained by;

$$\dot{m}_1 = \rho_{1o} \times V \times \frac{A_c}{2}$$

So,

$$\frac{\partial \dot{m}_1}{\partial \rho_{1o}} = V \times \frac{A_c}{2} \qquad \text{and} \qquad \frac{\partial \dot{m}_1}{\partial V} = \rho_{1o} \times \frac{A_c}{2}, \text{ then}$$

$$W_{\dot{m}_1} = \left[\left\{ \left(\frac{\partial \dot{m}_1}{\partial \rho_{1o}} \right)^2 \times \left(W_{\rho_{1o}} \right)^2 \right\} + \left\{ \left(\frac{\partial \dot{m}_1}{\partial V} \right)^2 \times (W_V)^2 \right\} \right]^{0.5} \qquad\qquad 5.4$$

- The air mass flow rate in the lower channel is obtained by;

$$\dot{m}_2 = \rho_{2o} \times V \times \frac{A_c}{2}$$

So,

$$\frac{\partial \dot{m}_2}{\partial \rho_{2o}} = V \times \frac{A_c}{2} \quad \text{and} \quad \frac{\partial \dot{m}_2}{\partial V} = \rho_{2o} \times \frac{A_c}{2}, \text{then}$$

$$W_{\dot{m}_2} = \left[\left\{ \left(\frac{\partial \dot{m}_2}{\partial \rho_{2o}} \right)^2 \times (W_{\rho_{2o}})^2 \right\} + \left\{ \left(\frac{\partial \dot{m}_2}{\partial V} \right)^2 \times (W_V)^2 \right\} \right]^{0.5} \qquad 5.5$$

- The uncertainty of the useful heat output from upper and lower channel $W_{\dot{q}_{u1,Ex}}, W_{\dot{q}_{u2,Ex}}$ is evaluated as follows:

  The useful heat output is a function of the air mass flow rate, the inlet air temperature and the outlet air temperature;

  $\dot{q}_{u1,Ex} = f\ (\dot{m}_1, T_{f1o},\ T_{f1i})$ and $\dot{q}_{u2,Ex} = f\ (\dot{m}_2, T_{f2o},\ T_{f2i})$.

- The useful heat output from upper channel is obtained by;

  $$\dot{q}_{u1,Ex} = \dot{m}_1 c_p (T_{f1o} - T_{f1i})$$

  So,

  $$\frac{\partial \dot{q}_{u1,Ex}}{\partial \dot{m}_1} = c_p (T_{f1o} - T_{f1i}) , \quad \frac{\partial \dot{q}_{u1,Ex}}{\partial T_{f1o}} = \dot{m}_1 c_p \text{ and } \frac{\partial \dot{q}_{u1,Ex}}{\partial T_{f1i}} = -\dot{m}_1 c_p \text{ , then}$$

  $$W_{\dot{q}_{u1,Ex}} = \left[\left\{ \left(\frac{\partial \dot{q}_{u1,Ex}}{\partial \dot{m}_1} \right)^2 \times (W_{\dot{m}_1})^2 \right\} + \left\{ \left(\frac{\partial \dot{q}_{u1,Ex}}{\partial T_{f1o}} \right)^2 \times (W_{T_{f1o}})^2 \right\} + \right.$$

  $$\left. \left\{ \left(\frac{\partial \dot{q}_{u1,Ex}}{\partial T_{f1i}} \right)^2 \times (W_{T_{f1i}})^2 \right\} \right]^{0.5}$$

  $$W_{\dot{q}_{u1,Ex}} = \left[\left\{ \left(c_p (T_{f1o} - T_{f1i}) \right)^2 \times (W_{\dot{m}_1})^2 \right\} + \left\{ (\dot{m}_1 c_p)^2 \times (W_{T_{f1o}})^2 \right\} + \right.$$

  $$\left. \left\{ (-\dot{m}_1 c_p)^2 \times (W_{T_{f1i}})^2 \right\} \right]^{0.5} \qquad 5.6$$

- The useful heat output from lower channel is obtained by;

  $$\dot{q}_{u2,Ex} = \dot{m}_2 c_p (T_{f2o} - T_{f2i})$$

  So,

  $$\frac{\partial \dot{q}_{u2,Ex}}{\partial \dot{m}_2} = c_p (T_{f2o} - T_{f2i}), \quad \frac{\partial \dot{q}_{u2,Ex}}{\partial T_{f2o}} = \dot{m}_2 c_p \quad \text{and} \quad \frac{\partial \dot{q}_{u2,Ex}}{\partial T_{f2i}} = -\dot{m}_2 c_p, \text{then}$$

$$W_{\dot{q}_{u2,Ex}} = \left[\left\{ \left(\frac{\partial \dot{q}_{u2,Ex}}{\partial \dot{m}_2} \right)^2 \times (W_{\dot{m}_2})^2 \right\} + \left\{ \left(\frac{\partial \dot{q}_{u2,Ex}}{\partial T_{f2o}} \right)^2 \times (W_{T_{f2o}})^2 \right\} + \left\{ \left(\frac{\partial \dot{q}_{u2,Ex}}{\partial T_{f2i}} \right)^2 \times (W_{T_{f2i}})^2 \right\} \right]^{0.5}$$

$$W_{\dot{q}_{u2,Ex}} = \left[\left\{ \left(c_p (T_{f2o} - T_{f2i}) \right)^2 \times (W_{\dot{m}_2})^2 \right\} + \left\{ (\dot{m}_2 c_p)^2 \times (W_{T_{f2o}})^2 \right\} + \left\{ (-\dot{m}_2 c_p)^2 \times (W_{T_{f2i}})^2 \right\} \right]^{0.5} \qquad 5.7$$

Table 5.3 shows the evaluated uncertainties of the parameters, that are used for calculating useful heat and the overall uncertainty in the useful heat. From the data given, it's found that the average of the uncertainty of the useful heat output from upper air channel and lower are;

$W_{\dot{q}_{u1,Ex}} = 83.24194 \ W = 27.25537 \ \%.$

$W_{\dot{q}_{u2,Ex}} = 87.1846 \ W = 24.54759 \ \%.$

Table 5.3: The evaluated uncertainties of the parameters that are used to calculate useful heat and the overall uncertainty in the useful heat.

Time	$T_{f1i} = T_{f2i}$ (K)	T_{f1o} (K)	T_{f2o} (K)	ρ_{1o} kg/m3	$W_{\rho_{1o}}$ kg/m3	$W_{\rho_{1o}}$ (%)	ρ_{2o} kg/m3	$W_{\rho_{2o}}$ kg/m3	$W_{\rho_{2o}}$ (%)	$\dot{m}_1$ (kg/s)	$W_{\dot{m}_1}$ (kg/s)	$W_{\dot{m}_1}$ (%)
11:00	290.083	292.583	292.633	1.20695	0.00204	0.16938	1.20675	0.00204	0.16935	0.10156	0.01391	13.6968
11:30	290.367	293.917	294.467	1.20152	0.00203	0.16882	1.1993	0.00202	0.16858	0.1011	0.01385	13.6968
12:00	291.15	294.85	295.55	1.19775	0.00202	0.16842	1.19493	0.00201	0.16813	0.10079	0.0138	13.6968
12:30	291.967	295.5	296.15	1.19513	0.00201	0.16815	1.19252	0.002	0.16787	0.10056	0.01377	13.6968
13:00	292.117	295.317	296.083	1.19587	0.00201	0.16823	1.19279	0.002	0.1679	0.10063	0.01378	13.6968
13:30	292.3	295.183	295.85	1.1964	0.00201	0.16828	1.19372	0.00201	0.168	0.10067	0.01379	13.6968
14:00	291.583	294.2	294.733	1.20037	0.00202	0.1687	1.19822	0.00202	0.16847	0.10101	0.01383	13.6968
14:30	291.067	293.683	294.017	1.20247	0.00203	0.16891	1.20112	0.00203	0.16877	0.10118	0.01386	13.6968

Time	$\dot{m}_2$ (kg/s)	$W_{\dot{m}_2}$ (kg/s)	$W_{\dot{m}_2}$ (%)	$\dot{q}_{u1,Ex}$ (W)	$W_{\dot{q}_{u1,Ex}}$ (W)	$W_{\dot{q}_{u1,Ex}}$ (%)	$\dot{q}_{u2,Ex}$ (W)	$W_{\dot{q}_{u2,Ex}}$ (W)	$W_{\dot{q}_{u2,Ex}}$ (%)
11:00	0.10154	0.01391	13.6968	253.899	79.7908	31.4261	258.933	80.0828	30.9279
11:30	0.10092	0.01382	13.6968	358.915	86.7616	24.1733	413.753	91.1238	22.0237
12:00	0.10055	0.01377	13.6968	372.905	87.6788	23.5124	442.411	93.4175	21.1156
12:30	0.10035	0.01374	13.6968	355.326	86.1698	24.2509	419.775	91.3255	21.7558
13:00	0.10037	0.01375	13.6968	322.006	83.7143	25.9978	398.119	89.5004	22.4808
13:30	0.10045	0.01376	13.6968	290.268	81.5357	28.0898	356.585	86.1985	24.1733
14:00	0.10082	0.01381	13.6968	264.303	80.0727	30.2958	317.598	83.5172	26.2965
14:30	0.10107	0.01384	13.6968	264.754	80.2119	30.2967	298.153	82.3111	27.6071

Chapter 6

CONCLUSION

The principal aim of the present work is to investigate the performance of a D-F/GVCPSAC which is intended to be used in an office for space heating during typical winter day in N. Cyprus. The performance of D-F/GVCPSAC is investigated experimentally and theoretically and below outcomes are achieved:

The first phase of the current work is to estimate the MEDC Office heating load by using Energy plus software. The simulation results revealed the daily average values of the building heating load for three months (November, December and January). The maximum heating load occurred in the coldest day of winter, sixteen of January as 4564 W.

The second outcome of this work is the evaluated number and the area necessary to cover the load of the office. This is achieved by evaluating the thermal performance of the collector. The thermal performance is investigated by simulations and measurements under the same environmental parameters that are obtained during 15th of December, from 09:20 until 16:00. The required number of collector and the area that is necessary to cover the target load is found by simulations as 6 collectors and 10 m^2. On the other hand, it is found from experimental investigation that, 9 collectors with 16 m^2 are required. It is seen that, there are disagreement between the simulation and experimental results. The disagreement is thought to be generated by

the following reasons;

- The exit air from the collector exposed directly to the ambient, which can reduce the exit air temperature, thus resulting in differences between the simulations and experiments.

- Thermal properties of all the materials that are employed for manufacturing the collector should be investigated in detail thus reducing the possible mismatch between the actual properties and those used for the calculations.

- The accuracies of the employed measuring equipment is generating significant uncertainties in the experimental results (up to 27 %, see section 5.3), thus equipment having better accuracies should be used.

Consequently nine of this particular solar collector can be coupled together for covering the heating demand of the considered office. It is also recommended that the simulations for obtaining the required number of collectors for covering the demand for the space should be used with care as they are resulting with higher useful heat which gives less number of collectors.

It is suggested that in any case an auxiliary heater should be employed for the days having not enough solar radiation.

REFERENCES

[1] T. Foley, T. Kane, H. Rainer, S. Sawyer, M. Sander, R. Taylor, S. Teske, H. Lehmann, M. Alers, and D. Hales, "Renewables 2015 global status report," pp. 1–251, 2015.

[2] IEA-ETSAP and IRENA, "Solar heating and cooling for residential applications - Technology brief," no. January, 2015.

[3] "kib-tek," *Production and Consumption Statistics*, 2016. [Online]. Available: https://www.google.com.cy/?gfe_rd=cr&ei=WQSiV7GBFMTb8AeJyreADA &gws_rd=ssl#q=kib-tek+kktc+elektrik+kurumu+2015+YILI. [Accessed: 03-Aug-2016].

[4] D. Aydin, S. P. Casey, and S. Riffat, "Theoretical analysis of the potential for thermochemical heat storage under Mediterranean climate conditions: Northern Cyprus Case," *Futur. Cities Environ.*, vol. 1, no. 1, p. 2, 2015.

[5] G. Makrides, B. Zinsser, G. E. Georghiou, M. Schubert, and J. H. Werner, "Potential of Photovoltaic Systems in Countries with High Solar Irradiation," pp. 1–6, 2008.

[6] A. Kahoorzadeh, S. Shahwarzi, E. Farjami, and S. Osivand, "Investigation of Usage of Passive Solar Energy in Salamis Road's Buildings, Famagusta," *Int. J. Environ. Sci. Dev.*, vol. 5, no. 2, pp. 132–136, 2014.

[7] L. Aldabbagha, F. Egelioglu, and M. Al-Khawajah, "The effect of partitioning single pass mesh wire packed bed solar air heater," *HEFAT 2010*, 2010.

[8] R. Sahebari, V. Eenesi, and U. Tamer, "Designing and Manufacturing of an Solar Air Heater," Eastern Mediterranean University.

[9] S. A. Kalogirou, *Solar thermal collectors and applications*, vol. 30, no. 3. 2004.

[10] R. Nowzaria, L. Aldabbagh, and N. Mirzaei, "EXPERIMENTAL STUDY ON DOUBLE PASS SOLAR AIR HEATER WITH MESH LAYERS AS ABSORBER PLATE*2013*",.

[11] T. (Izmir I. of T. Maraba, "An Experimental Study On Enhancement Of Heat Transfer In A Solar Air Heater Collector By Using Porous Medium," no. October, pp. 1–107, 2012.

[12] M. Hedayatizadeh, F. Sarhaddi, A. Safavinejad, F. Ranjbar, and H. Chaji, "Exergy loss-based efficiency optimization of a double-pass/glazed v-corrugated plate solar air heater," *Energy*, vol. 94, pp. 799–810, 2016.

[13] E. Sparrow and S. Lin, "Absorption of thermal radiation in a V-groove cavity," *Int. J. Heat Mass Transf.*, 1962.

[14] P. Wang, H. Guan, Z. Liu, and G. Wang, "High temperature collecting performance of a new all-glass evacuated tubular solar air heater with U-shaped tube heat exchanger," *Energy Convers. ..., 2014*.

[15] S. Budea, "Solar air collectors for space heating and ventilation applications-performance and case studies under Romanian climatic conditions," *Energies*, vol. 7, no. 6, pp. 3781–3792, 2014.

[16] M. Krzaczek and Z. Kowalczuk, "Thermal Barrier as a technique of indirect heating and cooling for residential buildings," *Energy Build.*, 2011.

[17] H. Chan, S. Riffat, and J. Zhu, "Review of passive solar heating and cooling technologies," *Renew. Sustain. Energy Rev.*, 2010.

[18] T. Schmidt, D. Mangold, and H. Müller-Steinhagen, "Central solar heating plants with seasonal storage in Germany," *Sol. energy*, 2004.

[19] H. Yeh and C. Ho, "Heat-transfer enhancement of double-pass solar air heaters with external recycle," *J. Taiwan Inst. Chem. Eng. 2011*.

[20] M. Ben-Amara, I. Houcine, A. Guizani, and M. Maalej, "Efficiency investigation of a new-design air solar plate collector used in a humidification–dehumidification desalination process," *Renew. Energy*, 2005.

[21] R. Karwa and K. Chauhan, "Performance evaluation of solar air heaters having v-down discrete rib roughness on the absorber plate," *Energy*, 2010.

[22] D. Alta, E. Bilgili, C. Ertekin, and O. Yaldiz, "Experimental investigation of three different solar air heaters: Energy and exergy analyses," *Appl. Energy*, 2010.

[23] K. Joudi and A. Farhan, "Greenhouse heating by solar air heaters on the roof," *Renew. Energy*, 2014.

[24] Bashria Abdrub alrasoul abdallah yousef and N. M. Adam, "PERFORMANCE ANALYSIS FOR V-GROOVE ABSORBER Bashria Abdrub alrasoul Abdallah Yousef * and Nor Mariha Adam," vol. 14, no. 1999, pp. 39–52, 2006.

[25] M. A. Karim, Z. M. Amin, and A. Almunasif, "Performance Comparison of Single and Double Pass Solar Air Collectors," no. May, pp. 435–444, 2014.

[26] D. Crawley and C. Pedersen, "EnergyPlus: energy simulation program," *ASHRAE ...*, 2000.

[27] R. Strand, R. Liesen, and M. Witte, "Resources for teaching building energy simulation," *Proc. SimBuild*, 2004.

[28] S. Wittkopf, A. Kambadkone, H. Quanhui, and N. Khai, "Development of a Solar Radiation and BIPV Design tool as EnergyPlus plugin for Google SketchUp," *Build. Simul.*, 2009.

[29] U. D. O. Energy, "EnergyPlus Engineering Reference: The Reference to EnergyPlus Calculations," *US Dep. Energy*, no. c, p. 1051, 2010.

[30] M. Ozdenefe and J. Dewsbury, "Thermal performance of a typical residential Cyprus building with phase change materials," *Build. Serv. Eng. ..., 2015*.

[31] T. Liu, W. Lin, W. Gao, and C. Xia, "A comparative study of the thermal performances of cross-corrugated and v-groove solar air collectors," *Int. J. Green Energy*, 2007.

[32] W. Lin, W. Gao, and T. Liu, "A parametric study on the thermal performance of cross-corrugated solar air collectors," *Appl. Therm. Eng.*, 2006.

[33] W. H. McAdams, *Heat transmission*. McGraw-Hill, 1954.

[34] S. P. Sukhatme and J. K. Nayak, *SOLAR ENERGY:Principles of Thermal Collection and Storage*. 2008.

[35] J. Duffie and W. Beckman, "Solar engineering of thermal processes *2013* ",.

[36] R. Verma, R. Chandra, and H. P. Garg, "Parametric studies on the corrugated solar air heaters with and without cover," *Renew. Energy*, vol. 1, no. 3–4, pp. 361–371, Jan. 1991.

[37] K. G. T. Hollands and E. C. Shewen, "Optimization of Flow Passage Geometry for Air-Heating, Plate-Type Solar Collectors," *J. Sol. Energy Eng.*, vol. 103, no. 4, p. 323, Nov. 1981.

[38] J. Hill and T. Kusuda, "Proposed standard method of testing for rating solar collectors based on thermal performance," *NSF/ERDA*, 1974.

[39] A. Standard, "93-77," *Methods Test. to Determ. Therm. …*, 1977.

[40] S. Singh and P. Dhiman, "Thermal performance of double pass packed bed solar air heaters–A comprehensive review," *Renew. Sustain. Energy Rev.*, 2016.

[41] "PASPORT-Fast-Response-Temperature-Probe-Manual-PS-2135.pdf." [Online].Available: https://www.pasco.com/file_downloads/Downloads_Manuals/PASPORT-Fast-Response-Temperature-Probe-Manual-PS-2135.pdf. [Accessed: 14-Dec-2016].

[42] S. Chow, E. Lee, and D. Li, "Short-term prediction of photovoltaic energy generation by intelligent approach," *Energy Build.*, 2012.

[43] J. P. Holman, *J.P. Holman*. .

[44] S. Kline and F. McClintock, "Describing uncertainties in single-sample experiments," *Mech. Eng. 1953*.

[45] "PASPORT Weather Anemometer Sensor - PS-2174: PASCO." [Online]. Available: https://www.pasco.com/prodCatalog/PS/PS-2174_pasport-weather-anemometer-sensor/. [Accessed: 01-Feb-2017].

APPENDIX

MATLAB CODE

```
                     % initial temperatures of each components of the(DPGVC);

Tg1= 296.0424;       % initial temperature of Upper Glass Cover;
Tg2= 318.2724;       % initial temperature of Lower Glass Cover;
Tf1= 322.2968;       % initial Air temperature in the Upper Channel;
Tap= 335.3370;       % initial temperature of the V-corrugated Absorber Plate;
Tf2= 323.4910;       % initial Air temperature in the Lower Channel;
Tbp=322.60461;       % initial temperature of the Flate Absorber Plate;


                     % Tg1(1)= input('Please enter the value of Tg1    ');
                     % Tg2(1)= input('Please enter the value of Tg2    ');
                     % Tf1(1)= input('Please enter the value of Tf1    ');
                     % Tap(1)= input('Please enter the value of Tap    ');
                     % Tf2(1)= input('Please enter the value of Tf2    ');
                     % Tbp(1)= input('Please enter the value of Tbp    ');
```

At 11:00

```
                     % Measured Values of Ambiant Parameters;
T_a=290.0833;        % Ambient temperature(K);
G=915.5238;          % Solar irradiance (based on Ah) (W/m2);
V_w=1.316667;        % Wind velocity (m/s);
```

Inserted data

```
Q_office=4564;       % The heating Load required for the Targeted building based on the
Energyplus Software Results;
T_s=T_a-6;           % the sky temperature;
g=9.8;               % gravitation;
Tau_g=0.9;           % Transmittance of the glass cover;
PI=3.141592654;      % Constant mathematical;
theta=45*PI/180;     % Tilt angle (Radian);
alpha_g=0.06;        % Absorptivity of the glass cover;
alpha_ap=0.9;        % Absorptivity of the V-corrugated absorber ;
E_g1=0.88;           % Emissivity of the upper glass cover;
E_g2=0.88;           % Emissivity of the lower glass cover;
E_ap=0.9;            % Emissivity of the V-corrugated absorber;
E_bp=0.9;            % Emissivity of the Flate absorber(back plate);
segma=5.668e-8;      % Stefan-Boltzmann constant;
L=1.95;              % Length of heater (m);
W=0.90;              % Width of heater (m);
A_h=L*W;             % Heater area   (m2);
A_a=2*L*W;           % Surface area of V-corrugated Absorber (m2);
H1=0.01;             % Thickness between the glass plates (m);
H2=0.1;              % Height of the Air Channel (m);
k_bp=79.5;           % Thermal conductivity of the Flat absorber (back plate);
k_wood=0.1;          % Thermal conductivity of the Wood (Wooden box);
k_ins=0.045;         % Thermal conductivity of the insulation plate (Foam);
k_Exc=79.5;          % Thermal conductivity of the out layer Cover (Galvanized Steel);
t_bp=0.002;          % Thickness of of the Flat absorber (back plate)(m);
```

```matlab
tins=0.02;          % Thickness of the insulation plate(Foam) (m);
t_wood=0.04;        % Thickness of Wood (Wooden box)(m);
t_Exc=0.002;        % Thickness of the out layer body Cover (Galvanized Steel)(m);
h_w=2.8+3*V_w;      % The convective heat transfer coefficient from the upper glass
cover due to wind;
mf=0.2;             % Total mass flow rate of air through heater (kg/s);
Cp=1000;            % Specific heat of air at constant pressure;
n=9;                % Number of separate flow passages experienced by air in series
through a collector array;
Dh=2*H2/3;          % Hydraulic diameter (m);

                    %  Note; Make it i=100 in fact the condition will be satisfied
after i=70

for i=1:10
                    % thermal expansion coefficient
beta=1/((Tg1+Tg2)/2);

                    % The radiative heat transfer coefficient from the upper glass
cover to sky

hr_g1s=segma*E_g1*(Tg1+T_s)*(Tg1^2 +T_s^2);

                    % Radiative heat transfer coefficient between the two glass covers

hr_g2g1=(segma*((power(Tg1,2) + power(Tg2,2))*(Tg1+Tg2)))/(1/E_g1 +1/E_g2-1);

                    % Density of the air trapped between the two glass covers

Ro= 3.9147 -(0.016082*((Tg2+Tg1)/2))+((2.9013e-5)*((Tg2+Tg1)/2)^2)-((1.9407e-
8)*(((Tg2+Tg1)/2)^3));

                    % Viscosity of the Air trapped between two glass covers

Mu=(1.6157+(0.06523*((Tg2+Tg1)/2))-(3.0297e-5*((Tg2+Tg1)/2)^2))*(10^(-6));

                    % Dynamic viscosity of the Air trapped between two glass
cover(m2/s)
v=Mu/Ro;

                    % Thermal conductivity of the Air trapped between two glass cover

k=(0.0015245+(0.097459*((Tg2+Tg1)/2)) -((3.3322e-5)*((Tg2+Tg1)/2)^2))*10^(-3);

                    % Prandtl number of the Air trapped between two glass cover

Pr=Mu*Cp/k;
                    % The Rayleigh number for air trapped  between the two glass
covers

Ra=(g*beta*Pr*(Tg2-Tg1)*H1^3)/(v^2);

a1=(1-(1708/(Ra*(cos(theta)))))*(0);

b1= 1-1708*((sin(1.8*theta))^1.6)/(Ra*cos(theta));

c1=(((Ra*(cos(theta))/5830)^(1/3))-1)*(0);
```

```matlab
                    % Nusselt number for air trapped  between the two glass
covers(valid for 0 < = theta = < 75)

Nu_g1g2=1+1.44*a1*b1+c1;

                    % The convective heat transfer coefficient for air trapped  between
the two glass covers

hc_g2g1=Nu_g1g2*k/H1;

                    % Viscosity of the Air in Upper channel

Mu_f1=(1.6157+(0.06523*Tf1)-(3.0297e-5*(Tf1)^2))*(10^-6);

                    % Reynolds number for the upper air passage

Re_f1=(2*mf/(3*Mu_f1*W))

                    % Nusselt number for air in the upper air passage ( valid for 2800
<Re < 10^4);

Nu_f1g2=1.9*(10^(-6))*((Re_f1)^1.76)+(112.5*(H2/L)*n);

                    % Thermal conductivity for the air in the upper passage;

k_f1=(0.0015245+(0.097459*Tf1) -((3.3322e-5)*Tf1^2))*10^-3;

                    % Convective heat transfer coefficient between upper channel
flowing air and Lower glass cover

hc_f1g2=Nu_f1g2*(k_f1/Dh);

                    % Radiative heat transfer coefficient between V-corrugated absorber
and Lower glass cover

hr_apg2=(segma*E_g2*E_ap*((power(Tap,2) + power(Tg2,2))*(Tap+Tg2)))/(E_g2
+E_ap+E_ap*E_g2);

                     % Nusselt number for upper channel flowing air ( valid for 2800
<Re < 10^4)

Nu_apf1=1.9*(10^(-6))*((Re_f1)^1.76)+(112.5*(H2/L)*n);

                    % Convective heat transfer coefficient between  upper channel
flowing air and V-corrugated absorber

hc_apf1=Nu_apf1*(k_f1/Dh);

                    %  Viscosity of the Air in Lower channel;

Mu_f2=(1.6157+(0.06523*Tf2)-(3.0297e-5*(Tf2)^2))*(10^-6);

                    % Reynolds number for the Lower air passage;

Re_f2=(2*mf/(3*Mu_f2*W))

                    % Thermal conductivity for air in the Lower passage;
k_f2=(0.0015245+(0.097459*Tf2) -((3.3322e-5)*Tf2^2))*10^-3;
```

76

```matlab
                    % Nusselt number for the air in the upper air passage ( valid for
2800 <Re < 10^4)

Nu_apf2=1.9*(10^(-6))*((Re_f2)^1.76)+(112.5*(H2/L)*n);

                    % Convective heat transfer coefficient between Lower channel
flowing air and V-corrugated absorber

hc_apf2=Nu_apf2*(k_f2/Dh);

                    % Nusselt number for Lower channel flowing air( valid for 2800 <Re
< 10^4);

Nu_f2bp=1.9*(10^(-6))*((Re_f2)^1.76)+(112.5*(H2/L)*n);

                     % Convective heat transfer coefficient between Lower channel
flowing air and Flat absorber(back plate)

hc_f2bp=Nu_f2bp*(k_f2/Dh);

                    % the radiative heat transfer coefficient between V-corrugated
absorber and back plates

hr_apbp=(segma*E_bp*E_ap*((power(Tap,2) + power(Tbp,2))*(Tap+Tbp)))/(E_bp
+E_ap+E_bp*E_ap);

                    % Total thermal resistance for back of the collector ;

R=(t_bp/k_bp)+(tins/k_ins)+(t_wood/k_wood)+(t_Exc/k_Exc)+(1/h_w);

                    % Total Thermal conductivity for bottom components of the collector;

hb=1/R;


%%%%%%%%%%%%%%%%%%%%%%%%%%%%%%%%%%%%%%%%%%%%%%%%%%%%%%%%%%%%%%%%%%%%%%%%%%%%%%%%%%%
                    % Expression Matrix of the energy balance equations

S11=hr_g2g1+hc_g2g1+h_w+hr_g1s;
S12=(hr_g2g1+hc_g2g1)*(-1);
S13=0;
S14=0;
S15=0;
S16=0;
S21=(hr_g2g1+hc_g2g1)*A_h*(-1);
S22=((hr_apg2*A_a)+(hc_f1g2+hr_g2g1+hc_g2g1)*A_h);
S23=hc_f1g2*A_h*(-1);
S24=(hr_apg2*A_a)*(-1);
S25=0;
S26=0;
S31=0;
S32=hc_f1g2*A_h*(-1);
S33=(hc_apf1*A_a)+(mf*Cp)+(hc_f1g2*A_h);
S34=(hc_apf1*A_a)*(-1);
S35=0;
S36=0;
```

```matlab
S41=0;
S42=(hr_apg2*A_a)*(-1);
S43=(hc_apf1*A_a)*(-1);
S44=(hr_apg2+hc_apf1+hc_apf2+hr_apbp)*A_a;
S45=(hc_apf2*A_a)*(-1);
S46=(hr_apbp*A_a)*(-1);
S51=0;
S52=0;
S53=0;
S54=(hc_apf2*A_a)*(-1);
S55=(hc_apf2*A_a)+(mf*Cp)+(hc_f2bp*A_h);
S56=(hc_f2bp*A_h)*(-1);
S61=0;
S62=0;
S63=0;
S64=(hr_apbp)*(-1);
S65=(hc_f2bp)*(-1);
S66=hb+hr_apbp+hc_f2bp;
D1=(alpha_g*G)+(h_w*T_a)+(hr_g1s*T_s);
D2=Tau_g*alpha_g*G*A_h;
D3=mf*Cp*T_a;
D4=(Tau_g*Tau_g*alpha_ap*G*A_h);
D5=(mf*Cp*T_a);
D6=(hb)*T_a;
SS=[S11,S12,S13,S14,S15,S16;
    S21,S22,S23,S24,S25,S26;
    S31,S32,S33,S34,S35,S36;
    S41,S42,S43,S44,S45,S46;
    S51,S52,S53,S54,S55,S56;
    S61,S62,S63,S64,S65,S66]
DD=[D1;D2;D3;D4;D5;D6]

TT=inv(SS)*DD;

 Tg1n= TT(1)
 Tg2n= TT(2)
 Tf1n= TT(3)
 Tapn= TT(4)
 Tf2n= TT(5)
 Tbpn=TT(6)
 if abs(Tg1n-Tg1) > 0.001
        Tg1=Tg1n
 elseif abs(Tg2n-Tg2) > 0.001
        Tg2=Tg2n
 elseif abs(Tf1n-Tf1) > 0.001
        Tf1=Tf1n
 elseif abs(Tf2n-Tf2) > 0.001
        Tf2=Tf2n
 elseif  abs(Tapn-Tap) > 0.001
        Tap=Tapn
 else
  abs(Tbpn-Tbp) > 0.001
        Tbp=Tbpn
 end

end
```

```
Re_f1 =

   7.6005e+03


Re_f2 =

   7.5792e+03


SS =

   19.4695   -7.8483         0         0         0         0
  -13.7737   69.9959  -47.6633   -8.5588         0         0
         0  -47.6633  342.9900  -95.3267         0         0
         0   -8.5588  -95.3267  208.2241  -95.5429   -8.7958
         0         0         0  -95.5429  343.3143  -47.7714
         0         0         0   -2.5059  -27.2202   30.7335


DD =

   1.0e+04 *

    0.3397
    0.0087
    5.8017
    0.1171
    5.8017
    0.0292


Tg1n =

  293.4629


Tg2n =

  295.1920


Tf1n =

  293.2205


Tapn =

  298.8166


Tf2n =

  292.9684


Tbpn =
```

```
    293.3507


Tg1 =

  293.4629


Re_f1 =

   7.6005e+03


Re_f2 =

   7.5792e+03


SS =

   19.3309   -7.7752         0         0         0         0
  -13.6455   69.8676  -47.6633   -8.5588         0         0
         0  -47.6633  342.9900  -95.3267         0         0
         0   -8.5588  -95.3267  208.2241  -95.5429   -8.7958
         0         0         0  -95.5429  343.3143  -47.7714
         0         0         0   -2.5059  -27.2202   30.7335


DD =

   1.0e+04 *

    0.3378
    0.0087
    5.8017
    0.1171
    5.8017
    0.0292


Tg1n =

  293.4923


Tg2n =

  295.2024


Tf1n =

  293.2223


Tapn =
```

298.8181

Tf2n =

292.9689

Tbpn =

293.3512

Tg1 =

293.4923

Re_f1 =

7.6005e+03

Re_f2 =

7.5792e+03

SS =

```
   19.3325    -7.7761          0          0          0          0
  -13.6470    69.8691   -47.6633    -8.5588          0          0
         0   -47.6633   342.9900   -95.3267          0          0
         0    -8.5588   -95.3267   208.2241   -95.5429    -8.7958
         0          0          0   -95.5429   343.3143   -47.7714
         0          0          0    -2.5059   -27.2202    30.7335
```

DD =

   1.0e+04 *

```
    0.3378
    0.0087
    5.8017
    0.1171
    5.8017
    0.0292
```

Tg1n =

293.4920

Tg2n =

295.2023

```
Tf1n =

  293.2223


Tapn =

  298.8181


Tf2n =

  292.9689


Tbpn =

  293.3512


Tg2 =

  295.2023


Re_f1 =

   7.6005e+03


Re_f2 =

   7.5792e+03


SS =

   18.6795   -7.1231         0         0         0         0
  -12.5010   67.8743  -47.6633   -7.7100         0         0
         0  -47.6633  342.9900  -95.3267         0         0
         0   -7.7100  -95.3267  207.3753  -95.5429   -8.7958
         0         0         0  -95.5429  343.3143  -47.7714
         0         0         0   -2.5059  -27.2202   30.7335


DD =

   1.0e+04 *

    0.3378
    0.0087
    5.8017
    0.1171
    5.8017
    0.0292
```

Tg1n =

  293.4221

Tg2n =

  295.1758

Tf1n =

  293.2234

Tapn =

  298.8353

Tf2n =

  292.9746

Tbpn =

  293.3577

Tg1 =

  293.4221

Re_f1 =

   7.6005e+03

Re_f2 =

   7.5792e+03

SS =

   18.6759   -7.1212   0   0   0   0
  -12.4977   67.8710   -47.6633   -7.7100   0   0
         0   -47.6633   342.9900   -95.3267   0   0
         0   -7.7100   -95.3267   207.3753   -95.5429   -8.7958
         0   0   0   -95.5429   343.3143   -47.7714
         0   0   0   -2.5059   -27.2202   30.7335

DD =

```
1.0e+04 *

  0.3378
  0.0087
  5.8017
  0.1171
  5.8017
  0.0292


Tg1n =

  293.4229


Tg2n =

  295.1761


Tf1n =

  293.2235


Tapn =

  298.8354


Tf2n =

  292.9746


Tbpn =

  293.3577


Tg2 =

  295.1761


Re_f1 =

  7.6005e+03


Re_f2 =

  7.5792e+03


SS =

  18.6752   -7.1205         0         0         0         0
```

```
    -12.4964   67.8688   -47.6633    -7.7091          0          0
          0   -47.6633   342.9900   -95.3267          0          0
          0    -7.7091   -95.3267   207.3744   -95.5429    -8.7958
          0          0          0   -95.5429   343.3143   -47.7714
          0          0          0    -2.5059   -27.2202    30.7335
```

DD =

   1.0e+04 *

    0.3378
    0.0087
    5.8017
    0.1171
    5.8017
    0.0292

Tg1n =

   293.4228

Tg2n =

   295.1760

Tf1n =

   293.2235

Tapn =

   298.8354

Tf2n =

   292.9746

Tbpn =

   293.3577

Tf1 =

   293.2235

Re_f1 =

   8.1680e+03

```
Re_f2 =

   7.5792e+03


SS =

   18.6752   -7.1205        0        0        0        0
  -12.4964   65.2296  -45.0241   -7.7091        0        0
         0  -45.0241  335.0723  -90.0482        0        0
         0   -7.7091  -90.0482  202.0959  -95.5429   -8.7958
         0        0        0  -95.5429  343.3143  -47.7714
         0        0        0   -2.5059  -27.2202   30.7335


DD =

   1.0e+04 *

    0.3378
    0.0087
    5.8017
    0.1171
    5.8017
    0.0292


Tg1n =

   293.4471


Tg2n =

   295.2397


Tf1n =

   293.1687


Tapn =

   298.9860


Tf2n =

   293.0243


Tbpn =

   293.4140
```

```
Tg1 =

  293.4471


Re_f1 =

   8.1680e+03


Re_f2 =

   7.5792e+03


SS =

   18.6765   -7.1212         0         0         0         0
  -12.4976   65.2308  -45.0241   -7.7091         0         0
         0  -45.0241  335.0723  -90.0482         0         0
         0   -7.7091  -90.0482  202.0959  -95.5429   -8.7958
         0         0         0  -95.5429  343.3143  -47.7714
         0         0         0   -2.5059  -27.2202   30.7335


DD =

   1.0e+04 *

    0.3378
    0.0087
    5.8017
    0.1171
    5.8017
    0.0292


Tg1n =

  293.4468


Tg2n =

  295.2396


Tf1n =

  293.1687


Tapn =

  298.9860


Tf2n =
```

```
    293.0243


Tbpn =

    293.4140


Tg2 =

    295.2396


Re_f1 =

    8.1680e+03


Re_f2 =

    7.5792e+03


SS =

   18.6782   -7.1229         0         0         0         0
  -12.5006   65.2360   -45.0241   -7.7113         0         0
         0   -45.0241  335.0723  -90.0482         0         0
         0    -7.7113   -90.0482  202.0982  -95.5429   -8.7958
         0         0         0   -95.5429  343.3143  -47.7714
         0         0         0    -2.5059  -27.2202   30.7335


DD =

   1.0e+04 *

    0.3378
    0.0087
    5.8017
    0.1171
    5.8017
    0.0292


Tg1n =

    293.4470


Tg2n =

    295.2396


Tf1n =
```

293.1687

Tapn =

298.9859

Tf2n =

293.0243

Tbpn =

293.4140

Tf1 =

293.1687

Re_f1 =

8.1691e+03

Re_f2 =

7.5792e+03

SS =

```
   18.6782    -7.1229          0          0          0          0
  -12.5006    65.2310   -45.0191    -7.7113          0          0
         0   -45.0191   335.0573   -90.0382          0          0
         0    -7.7113   -90.0382   202.0882   -95.5429    -8.7958
         0          0          0   -95.5429   343.3143   -47.7714
         0          0          0    -2.5059   -27.2202    30.7335
```

DD =

   1.0e+04 *

```
    0.3378
    0.0087
    5.8017
    0.1171
    5.8017
    0.0292
```

Tg1n =

293.4470

```
Tg2n =

    295.2398


Tf1n =

    293.1686


Tapn =

    298.9862


Tf2n =

    293.0244


Tbpn =

    293.4141


Tf2 =

    293.0244
```

```
T_f1out=(2*Tf1n)-T_a           % Outlet air temperature from upper channel

q_u1=mf*Cp*(T_f1out-T_a)/2     % The useful energy gain by air flowing through the
upper passage

T_f2out=(2*Tf2n)-T_a           % Outlet air temperature from Lower channel

q_u2=mf*Cp*(T_f2out-T_a)/2     % The useful energy gain by air flowing through the
lower passage

Q_total=q_u1+q_u2              % The total useful energy gain output

Numb_C=Q_office/Q_total        % Number of  the air collector required to meet Targed
Heating Load

A_total=A_h*Numb_C             % Total required area of the solar air heaters to meet
Targed Heating Load

Eta=(Q_total/(G*A_h))*100      %the thermal efficiency of the collector
```

```
T_f1out =

    296.2538
```

```
q_u1 =

   617.0532


T_f2out =

   295.9655


q_u2 =

   588.2228


Q_total =

   1.2053e+03


Numb_C =

    3.7867

A_total =

    6.6456

Eta =

   75.0136
```
Investigation of the air velocity range

```
Ro_f1= 3.9147 -(0.016082*(T_f1out))+((2.9013e-5)*(T_f1out)^2)-((1.9407e-
8)*((T_f1out)^3));
V_f1=(Re_f1*Mu_f1)/(Ro_f1*Dh)
Ro_f2= 3.9147 -(0.016082*(T_f2out))+((2.9013e-5)*(T_f2out)^2)-((1.9407e-
8)*((T_f2out)^3));
V_f2=(Re_f2*Mu_f2)/(Ro_f2*Dh)
```

```
V_f1 =

    1.8641

V_f2 =

    1.8623
```

Published with MATLAB® R2013a